AJAE

Open Access

Vol. 16, No. 4, pp. 2022119, December 2022
doi: https://doi.org/10.5572/ajae.2022.119
ISSN (Online) 2287-1160, ISSN (Print) 1976-6912

Research Article

A Box-Model Simulation of the Formation of Inorganic Ionic Particulate Species and Their Air Quality Implications in Republic of Korea

Haeju Lee[1)], Dongwan Kim[1)], Minseung Yeo[1)], Yusin Kim[1)], Chang Hoon Jung[2)], Seogju Cho[3)], Ji Hoon Park[4)], Hye Jung Shin[4)], Sung Hoon Park[1),5),*]

[1)]Department of Environmental Engineering, Sunchon National University, Suncheon, Republic of Korea
[2)]Department of Health Management, Kyungin Women's University, Incheon, Republic of Korea
[3)]Research Institute of Public Health and Environment, Seoul Metropolitan Government, Seoul, Republic of Korea
[4)]Department of Air Quality Research, National Institute of Environmental Research of Korea, Incheon, Republic of Korea
[5)]The Research Institute for Sanitation and Environment of Coastal Areas, Sunchon National University, Suncheon, Republic of Korea

***Corresponding author.**
Tel: +82-61-750-3816
E-mail: shpark@scnu.ac.kr

Received: 2 December 2022
Revised: 15 December 2022
Accepted: 15 December 2022

ABSTRACT The Observation-Constrained Atmospheric BOX model (OCABOX) was used to analyze the formation of secondary inorganic PM species in the Seoul Metropolitan Area (SMA), South Korea. The measurement data of the ionic components of $PM_{2.5}$ and their gaseous precursors made at the Olympic Park ground site (37.53°N, 127.12°E) during the Korea-United States Air Quality field campaign were used to run OCABOX in observation-based mode and compare the simulation results. The use of the HNO_3 concentrations measured at a marine background site as the boundary conditions appeared to increase the accuracy of the model prediction of HNO_3 and particulate NO_3^- concentrations. For the primary precursors emitted considerably throughout the SMA, such as NO_x and NH_3, using the data measured inside the SMA as the boundary conditions could lead to more accurate predictions. OCABOX was shown to be a reliable tool to analyze the formation of secondary inorganic aerosol in the SMA if used with appropriate regional background concentrations and observation-based constraints

KEY WORDS Atmospheric box model, Inorganic ionic species, Secondary particulate matter, Nitrate, Gas-to-particle conversion

1. INTRODUCTION

Nitrate (NO_3^-) is an important secondary inorganic ionic particulate matter (PM) species produced by the oxidation of nitrogen oxides (NO_x). The chemical pathway from NO_x via nitric acid (HNO_3) to particulate nitrate is complicated (Seinfeld and Pandis, 2016) and is affected by other atmospheric species, such as VOCs (Meng *et al.*, 1997). In addition, the partitioning of total nitric acid (HNO_3+ NO_3^-) determined by the equilibrium between gaseous HNO_3 and particulate NO_3^- changes depending on temperature, relative humidity, and the concentrations of basic components, such as ammonia (NH_3), crustal species, and sea salt (Kim *et al.*, 2004; Ro *et al.*, 2001), that can neutralize HNO_3, whereas the total sulfuric acid ($H_2SO_4 + SO_4^{2-}$) exists primarily as particulate SO_4^{2-}. Therefore, the NO_3^- concentration varies considerably depending on the location and season.

Particulate NO_3^- can be a dominant ionic species in $PM_{2.5}$ where the ammonia

concentration is high enough to neutralize both sulfuric acid and nitric acid (Wang *et al.*, 2020), whereas it is usually present in the coarse mode where the ammonia concentration is insufficient (Ocskay *et al.*, 2006; Wolff, 1984; Savoie and Prospero, 1982). NO_x and NH_3 emissions are not being controlled very well in East Asia, including South Korea, compared to that of SO_2 (He *et al.*, 2007; Richter *et al.*, 2005), which may lead to an environment favorable to the formation of particulate ammonium nitrate (NH_4NO_3), frequently making NO_3^- the most abundant ionic particulate species (Kim *et al.*, 2017; Lee *et al.*, 2016; Park *et al.*, 2013; Shon *et al.*, 2012; Park and Kim, 2004; Choi *et al.*, 2001). The formation of NH_4NO_3 often coincides with the occurrence of high $PM_{2.5}$ concentration (Wang *et al.*, 2020; Park and Kim, 2004). One study reported that the particulate NO_3^- concentration in Seoul, Korea increased in the 2010s despite the decreasing gaseous NO_x concentration (Han and Kim, 2015), which warrants scientific understanding.

Together with laboratory experiments and ambient observations, modeling is one of the three principal tools for understanding atmospheric chemistry (Abbatt *et al.*, 2014). The use of atmospheric chemistry models plays an important role in interpreting the ambient observations and smog chamber measurements and designing new observations and experiments (Burkholder *et al.*, 2017; Wolfe *et al.*, 2016). In particular, 0-dimensional box models enable researchers to analyze the atmospheric chemistry intensively and compare various chemical mechanisms by focusing on the chemical conversions of air pollutants rather than on their transports (Sommariva *et al.*, 2020; Wolfe *et al.*, 2016). Understanding the major chemical pathways of secondary air pollutants, such as ozone and secondary inorganic PM species, is important for developing effective environmental policies (Kim and Lee, 2018). For this reason, box models have widely been used to interpret ambient measurements (Brune *et al.*, 2016; Whalley *et al.*, 2016; Edwards *et al.*, 2014; Lu *et al.*, 2012; Elshorbany *et al.*, 2009; Emmerson *et al.*, 2007; Carslaw *et al.*, 1999; Eisele *et al.*, 1994), chamber experiments (Novelli *et al.*, 2018; Chen *et al.*, 2015; Metzger *et al.*, 2008; Bloss *et al.*, 2005; Carter, 1995), and onboard measurements using aircrafts or ships (Sommariva *et al.*, 2011a, b, 2009, 2008; Ren *et al.*, 2008; Chen *et al.*, 2005; von Glasow *et al.*, 2003; Song *et al.*, 2003; Brauers *et al.*, 2001).

Box models are also helpful for investigating the causes of high air pollution events. Xue *et al.* (2014) examined a wintertime high-NO_3^- episode in Hong Kong using an observation-based box model and reported that both the gas-phase oxidation of NO_2 by OH radicals and heterogeneous N_2O_5 hydrolysis contributed to HNO_3 production, which in turn was converted to particulate NO_3^- under ammonia-rich conditions. However, Xue *et al.* (2014) used their box model only for diagnostic purposes; they reported only the reaction rates producing gaseous HNO_3 calculated from the measured data. Schroeder *et al.* (2020) used a box model to investigate the ozone production rate in the Seoul Metropolitan Area (SMA).

The strength of box models lies in their outstanding time efficiency stemming from the neglection or simplification of horizontal and vertical transports. The neglect of transport can be justified in the cases of extreme air stagnation. When the transport is considered using user-defined boundary conditions, the effects of boundary conditions on predicted pollutant concentrations may become considerable. For this reason, box models are generally used for "gaining conceptual understanding and testing hypotheses through targeted sensitivity simulations and comparison with observations" (Wolfe *et al.*, 2016) rather than for obtaining accurate predictions.

In the present work, a box model called the Observation-Constrained Atmospheric BOX model (OCA BOX), developed by modifying a three-dimensional (3D) chemical transport model EPA Models-3 Community Multiscale Air Quality Modeling System (CMAQ), was used to study the formation of secondary inorganic PM species in South Korea, where high PM concentrations are frequently associated with high concentrations of inorganic ionic species. The $PM_{2.5}$ concentration tends to be higher in winter and spring than in summer and fall because of higher emissions and poorer dispersion (in winter) or because of the long-range transport effects and intensive photochemical production of secondary species (in spring) (Kim *et al.*, 2018; Kim *et al.*, 2017; Kim *et al.*, 2014). This study examined the formation pathways of NO_3^- and its contribution to the high pollution events using measured data and box modeling.

2. MATERIALS AND METHODS

2.1 Measurement Data

Data on gaseous and particulate species concentra-

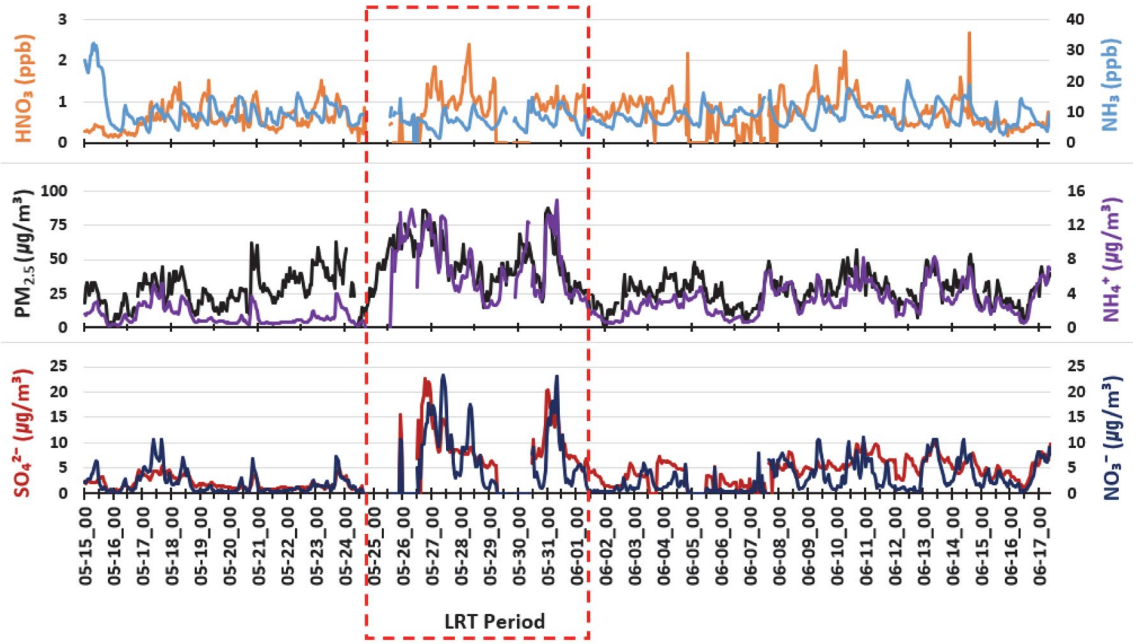

Fig. 1. Overview of the time evolutions of the concentrations of several key pollutants during the studied period.

tions and meteorological parameters are required to run and validate OCABOX. The Korea-United States Air Quality (KORUS-AQ) field study conducted jointly by the National Institute of Environmental Research of South Korea and the National Aeronautics and Space Administration of the United States in May–June 2016 offered extensive data sets measured from ground stations, aircrafts, and ships (Crawford *et al.*, 2021). The collected data have been used by many researchers trying to understand the factors influencing the air quality of Korea (e.g., Kim *et al.*, 2022; Park *et al.*, 2021; Jordan *et al.*, 2020; Oak *et al.*, 2019; Kim *et al.*, 2018; Nault *et al.*, 2018) because the KORUS-AQ campaign provided unprecedented comprehensive measurements of air pollutants, including both gas- and particulate-phase species.

In this study, a set of hourly data on major ionic components of $PM_{2.5}$, including NH_4^+, Na^+, K^+, Ca^{2+}, Mg^{2+}, NO_3^-, SO_4^{2-}, and Cl^-, and their gaseous precursors, such as HCl, SO_2, NO_x, HNO_3, and NH_3, measured at the Olympic Park (OP) ground site (37.53°N, 127.12°E) from 15 May to 17 June 2016 by Seoul Metropolitan Government Research Institute of Public Health and Environment (Choi *et al.*, 2019) were used to run OCABOX in the observation-based mode and to compare the simulation results. The $PM_{2.5}$ mass concentration was measured using a radiometric particulate mass monitor, FH62C14 (Thermo Scientific, USA), whereas a Monitor for Aerosol & Gasses in Ambient Air, MAR GA ADI 2080 (Metrohm Applikon., Netherlands), was used to determine the concentrations of the ionic particulate species and related gaseous species HCl, NH_3, and HNO_3. Gas species analyzers were used to measure the CO (Ecotech model EC9830, Australia), O_3 (Ecotech model EC9810, Australia), SO_2 (Ecotech model EC9850, Australia), and NO_x (Ecotech model EC9841, Australia) concentrations. One can refer to the literature (Choi *et al.*, 2019; Ghosh *et al.*, 2012) for more detailed information on the measurement and data processing methods. Meteorological parameters, such as air temperature, relative humidity, and wind speed, were also measured at the OP site.

Fig. 1 shows the concentrations of several key pollutants measured during the period. There was a distinct event exceeding the Korean daily $PM_{2.5}$ standard (35 μg/m^3) during 25–31 May, which will be called the LRT period because it was caused by enhanced long-range transport, and several relatively short events during which local emissions dominated due to stagnant air (Park *et al.*, 2021; Peterson *et al.*, 2019; National Institute of Environmental Research and National Aeronautics and Space Administration, 2017). During the KORUS-

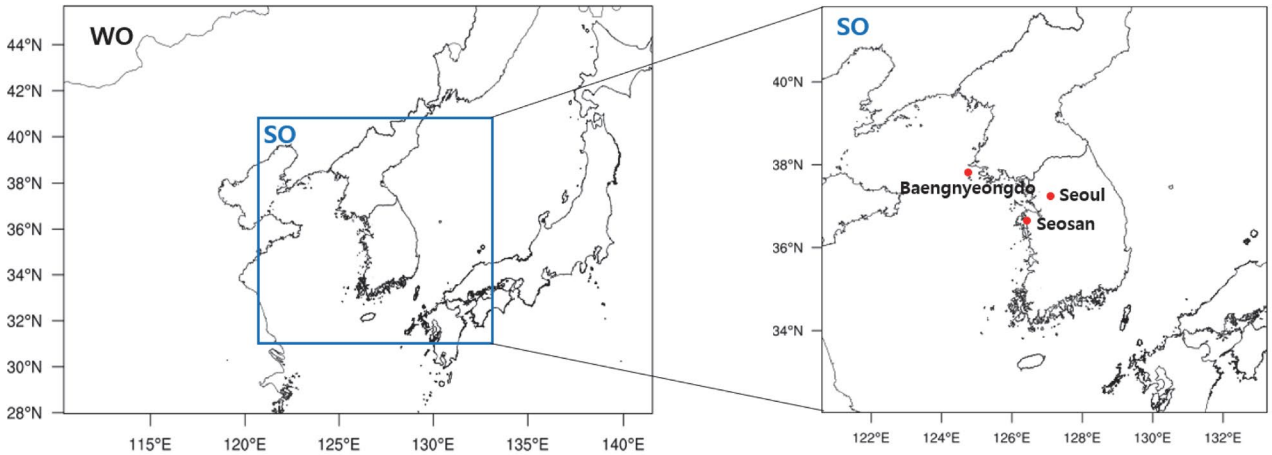

Fig. 2. Model domains for preparing meteorology and emissions inputs: the WRF domain (WO) and the SMOKE domain (SO).

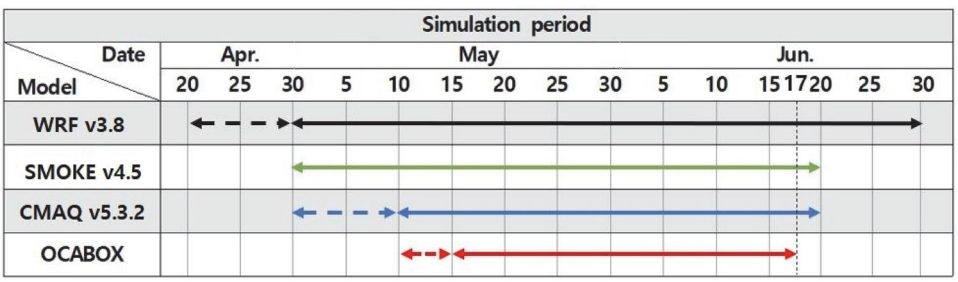

Fig. 3. Simulation periods of the models used. CMAQ was run only for supplying the average ratios $[NH_3]/[NH_4^+]$ and $[HNO_3]/[NO_3^-]$ in SA3.

AQ campaign, the air quality of Seoul was reportedly influenced strongly by the formation of secondary PM (Park *et al.*, 2021; Nault *et al.*, 2018; Kim *et al.*, 2018). This is supported by the high correlations among the $PM_{2.5}$ and ionic species concentrations shown after 25 May.

As shown in Section 3, the supply of appropriate regional background concentrations appeared to be important for the reliable operation of OCABOX. The data measured at a marine background site in Baengnyeong Island (BI) (37.97°N, 124.63°E) collected during the same period were provided as the regional background concentrations in several sensitivity analyses. The Beta Attenuation Monitor Model 1020 (BAM1020) (Met One Ins., USA) was used to measure the $PM_{2.5}$ mass concentration, whereas the anion and cation particle and gas system, AIM URG-9000D (URG Corporation, USA), was used to measure the ionic species in $PM_{2.5}$. The measured data of several gaseous species, CO (TELEDYNE API model T300, USA), O_3 (TELEDYNE API model T400, USA), SO_2 (TELEDYNE API model 100A, USA), and NO_2 (TELEDYNE API model T200, USA), were also used.

2.2 Operation of OCABOX

A box model OCABOX, developed by modifying the 3D chemical transport model CMAQ v.5.3.2 into 0-dimensional box model, was used in this study. Carbon Bond 6 (CB6) (Yarwood *et al.*, 2010) was used as the gas-phase mechanism and the 6th generation aerosol module (AERO6) was used as the aerosol mechanism including aqueous-phase and heterogeneous reactions. The horizontal dimension of the box was set at 30 km and the planetary boundary layer height (PBLH) predicted by a mesoscale meteorological model Weather Research and Forecasting (WRF) v3.8 (Powers *et al.*, 2017), which can be a proxy of the mixing layer height (MLH) (Banks *et al.*, 2015), was used as the vertical dimension of the box.

The meteorological input file was generated using the

Table 1. Information on the domain and physics options used for WRF running.

Model attributes	WRF v3.8
Domain (Horizontal grid)	Korea (81 × 61)
Horizontal resolution	30 km
Land use data	IGBP-Modified MODIS 20-category
Microphysics	WRF Single-Moment 6-class
Longwave radiation	RRTMG
Shortwave radiation	RRTMG
Land surface scheme	Pleim-Xiu
Planetary boundary layer	ACM2 PBL
Cumulus parameterization	Kain-Fritsch
Eta levels	1.000, 0.993, 0.983, 0.970, 0.954, 0.934, 0.909, 0.880, 0.832, 0.784, 0.735, 0.687, 0.604, 0.528, 0.232, 0.065, 0.048, 0.033, 0.020, 0.009, 0.000
Map projection	Lambert Conformal
Initial data	ERA-Interim Project (da627.0)

Table 2. SMOKE configuration used in this study.

Model attributes	SMOKE v4.5
Domain (Horizontal grid)	South Korea (35 × 35)
Horizontal resolution	30 km
Chemical mechanism	CB6
Emissions inventory	CAPSS 2016

output of WRF and measured data. Fig. 2 shows the WRF domain (WO) with a horizontal grid size of 30 km on a Lambert Conformal map projection covering the whole Korean Peninsula. The terrain-following sigma vertical coordinate was employed with 29 unevenly spaced vertical levels ranging from the surface to 50 hPa. ERA-Interim reanalysis data were used for the initial and boundary conditions. WRF was run from 0000 UTC 20 April to 0000 UTC 30 June 2016 (Fig. 3). The first 10 days of WRF simulation were treated as spin-up time, and only the fields from 0000 UTC 30 April were supplied to OCABOX simulations. Table 1 provides detailed information of the WRF domain and physics options used for the WRF run. The measured data for air temperature, relative humidity, and wind speed were overwritten to the WRF output file to replace the model prediction.

The emission fields for the OCABOX run were generated using Sparse Matrix Operator Kernel Emissions (SMOKE) v4.5. The Korean national emissions inventory called Clean Air Policy Support System (CAPSS) for 2016 (National Institute of Environmental Research, 2019) was used as the raw emissions data. The natural emissions were determined using the Model of Emissions of Gases and Aerosols from Nature (MEGAN) v2.1. Emissions speciation was performed using the chemical mechanism CB6. SMOKE was run from 0000 UTC 30 April to 0000 UTC 20 June 2016 (Fig. 3).

Table 2 summarizes the SMOKE run configuration used in this study. Fig. 2 shows the domain for the SMOKE run (SO).

OCABOX was run from 0000 UTC 10 May to 0000 UTC 17 June 2016, including a five-day spin-up (Fig. 3) for the five scenarios shown in Table 3: a base run (BASE) and four sensitivity analysis runs (SA1, SA2, SA3, and SA4). For the initial condition, the "profile" concentrations provided by the 3D model CMAQ were used. The profile concentrations were also used as the boundary conditions except for the species for which the concentrations measured at the BI marine background site (Na^+, K^+, Ca^{2+}, Mg^{2+}, Cl^-, SO_4^{2-}, NO_3^-, NH_4^+, NH_3, and HNO_3) were used, as shown in Table 3. For the build-up of the species whose concentrations are not measured at the OP site during the episode periods, the first five days of the OCABOX simulations were taken as the spin up time. Fig. 3 presents the simulation time set for the models used in this study.

CMAQ v5.3 was needed to generate the species concentrations at the BI site to perform a sensitivity test for the marine background concentrations, which will be explained in Section 3.4. WRF v3.8 was used as the meteorological driver for this test. Fig. S1 shows the spatial domains used for WRF (WC1 and WC2) and CMAQ (C1 and C2) simulations for this test. Two-way nesting between Domain 1 (WC1 and C1) and Domain 2 (WC2 and C2) was used. A Lambert Conformal map projection was employed for all domains. Table 4 and Table 5 show detailed information on the run configurations for WRF and CMAQ, respectively, used for this sensitivity test. WRF was run from 0000 UTC 20 April to 0000 UTC 20 June 2016, whereas CMAQ was run from 0000 UTC 30 April to 0000 UTC 20 June, with the first 10 days for both WRF and CMAQ runs treated as spin-up time. The emission fields were prepared for the domain C2 in the same way described above.

Table 3. Simulation conditions for the base and sensitivity test runs.

Model runs	Constraint (CSTR) species	Background (BCON) species measured at BI site	Comments
BASE	CO, O_3, SO_2, SO_4^{2-}, Na^+, K^+, Ca^{2+}, Mg^{2+}, Cl^-, HCl	CO, O_3, SO_2, NO_2	Base run
SA1	CO, O_3, SO_2, SO_4^{2-}, Na^+, K^+, Ca^{2+}, Mg^{2+}, Cl^-, HCl	CO, O_3, SO_2, NO_2	Emissions of NO_x and NH_3 doubled
SA2	CO, O_3, SO_2, SO_4^{2-}, Na^+, K^+, Ca^{2+}, Mg^{2+}, Cl^-, HCl, NH_3, NH_4^+, NO, NO_2	CO, O_3, SO_2, NO_2	NH_3, NH_4^+, NO, NO_2 added to constraint
SA3	CO, O_3, SO_2, SO_4^{2-}, Na^+, K^+, Ca^{2+}, Mg^{2+}, Cl^-, HCl	CO, O_3, SO_2, NO_2, Na^+, K^+, Ca^{2+}, Mg^{2+}, Cl^-, SO_4^{2-}, NO_3^-, NH_4^+, NH_3, HNO_3	Na^+, K^+, Ca^{2+}, Mg^{2+}, Cl^-, SO_4^{2-}, NO_3^-, NH_4^+, NH_3, and HNO_3 measured at BI site added to background concentrations
SA4	CO, O_3, SO_2, SO_4^{2-}, Na^+, K^+, Ca^{2+}, Mg^{2+}, Cl^-, HCl	CO, O_3, SO_2, Na^+, K^+, Ca^{2+}, Mg^{2+}, Cl^-, SO_4^{2-}, NO_3^-, HNO_3, NH_3, NH_4^+, NO, NO_2	Na^+, K^+, Ca^{2+}, Mg^{2+}, Cl^-, SO_4^{2-}, NO_3^-, and HNO_3 measured at BI site and NH_3, NH_4^+, NO, and NO_2 measured at OP site added to background concentrations

Table 4. WRF configurations used for the sensitivity test for background concentrations.

Model attributes	WRF v3.8	
Domain (Horizontal grid)	Domain1 East Asia (143 × 181)	Domain2 Korea (94 × 79)
Horizontal resolution	27 km	9 km
Nesting	Two-way	
Initial data	ERA-Interim Project (da627.0)	

Table 5. CMAQ configurations used for the sensitivity test for background concentrations.

Model attributes	CMAQ v5.3.2	
Domain (Horizontal grid)	Domain1 East Asia (128 × 174)	Domain2 Korea (82 × 67)
Horizontal resolution	27 km	9 km
Chemical mechanism	cb6r3_ae7_aq	

3. RESULTS AND DISCUSSION

The concentrations of all the species except NH_3, NH_4^+, NO, NO_2, HNO_3, and NO_3^- measured at the OP site were used as the constraints for the basis of the OCABOX run. For the missing data, the average values of the previous and next hours (in the cases of isolated missing data) or the average values for the whole simulation period (in the cases of consecutive missing data) were used in principle. On the other hand, this method could not be applied to Na^+, K^+, Ca^{2+}, and Mg^{2+} because there were too many missing values. In particular, there were only six samples that provided valid Na^+ concentrations. However, the average Na^+ concentration of those six samples was 0.46 μg/m^3, which is similar to the values reported previously for Seoul (Choi and Kim, 2010; Kang *et al.*, 2006, 2004; Lee *et al.*, 2005). For these cations, the average values of the measured concentrations were used for the whole simulation period.

Table 6 lists the average values measured for those cations. An anion Cl^- and gas species HCl are shown together. These six species are measured only occasionally (e.g. during intensive campaigns like the present study) in Korea and, therefore, box models often have to be run without their measured concentrations. Although the concentrations of these species are not very high, the possible errors due to the lack of information on their concentrations need to be estimated for wide applications of OCABOX. For the species whose concentrations are not constrained, the OCABOX calculates their concentrations by solving the governing mass balance equations with the initial and boundary conditions pro-

Table 6. Measured and profile values for the crustal and sea-salt species and related gas species concentrations.

Species	CMAQ profile values	Measurement average
Na^+ (μg/m^3)	0.44	0.46
Ca^{2+} (μg/m^3)	0.050	0.12
Mg^{2+} (μg/m^3)	0.058	0.060
K^+ (μg/m^3)	0.036	0.16
Cl^- (μg/m^3)	0.24	0.17
HCl (ppb)	0.14	0.15

vided from the "profile" values. Inherited from the 3D model CMAQ, the profile values represent the minimal background concentrations. Table 6 also lists the profile values for the six species. The differences between the profile values and measured ones are not very large; all the species showed agreement within a factor of two except for Ca^{2+} and K^+ because the concentrations of the crustal and sea-salt species in fine particles ($PM_{2.5}$) are not very high in the SMA except in the Asian dust transport periods.

A sensitivity test was conducted on the concentration input for the above-shown six species. The differences between the concentrations of HNO_3, NH_3, NO_3^-, and NH_4^+ calculated by OCABOX with and without the constraints for the six species listed in Table 6 were all less than 6%. The simulation without the constraints for the six species resulted in the increased concentrations of HNO_3 (by 5.1%) and NH_4^+ (by 5.9%) and decreased concentrations of NO_3^- (by 1.5%) and NH_3 (by 4.8%) because the profile values for the cations were lower than the measured ones while the profile value for Cl^- was higher than the measured one. These differences, however, are relatively small compared to the overall uncertainty of the OCABOX simulations. Hence, using the CMAQ profile as the initial and boundary conditions for these species can be justified when the measured data are not available. A previous study also showed that the effects of the crustal cations and Na^+ on the aerosol thermodynamics were very small (Kim *et al.*, 2022).

In the following subsections, the predictions of OCA BOX are compared with observations. The two secondary inorganic ionic aerosol species NO_3^- and NH_4^+ that were not constrained by observations and their gaseous precursors NO, NO_2, HNO_3, and NH_3 are the target species in the comparisons.

3.1 Base Run (BASE)

As shown in Table 3, the CO, O_3, SO_2, SO_4^{2-}, Na^+, K^+, Ca^{2+}, Mg^{2+}, Cl^-, and HCl concentrations measured at the OP site were used as constraints and the CO, O_3, SO_2, and NO_2 concentrations measured at the BI site were used as regional background conditions for the BASE simulation.

Fig. 4 compares the OCABOX-predicted concentrations with observations. The results of the integrated process rate (IPR) analysis, which is a part of the process analysis (PA), indicating the effects of each process, such as gas-phase chemistry (CHEM), horizontal advection (HADV), vertical diffusion (VDIF), emission (EMIS), dry deposition (DDEP), and aerosol processes (AERO), on the species concentrations are shown together. NO was supplied mostly by emission and converted to NO_2 via chemistry (Fig. 4a), whereas NO_2 was produced from the chemical reaction of NO and removed by chemistry and horizontal advection (Fig. 4b). Compared to the observations, both NO and NO_2 were underestimated by OCABOX considerably. The reason for underpredicting NO and NO_2 may be either the underestimation of NO_x emissions or too low background concentrations provided by the CMAQ profile, as was indicated by the huge effect of HADV on NO_2. This will be discussed in more detail in the following subsections presenting the sensitivity analysis results.

HNO_3 (Fig. 4c) and NH_3 (Fig. 4e) were also underpredicted, but the aspects were quite different; the underprediction of HNO_3 was remarkable mostly at night, whereas NH_3 was underpredicted during the day. The characteristic evolutions of NH_3 concentration and the emission rate (Fig. 4e) stem from the diurnal variation of mixing height (not shown); the low mixing height at night leads to a strong influence of emission, and the opposite is the case during the day. Regarding HNO_3, the story becomes completely different because HNO_3 is not a primary pollutant; the underestimation of HNO_3 is prominent at night.

During the day, HNO_3 is produced by

$$NO_2 + OH \rightarrow HNO_3 \quad (1)$$

whereas during the night, its production takes place via the following reactions:

$$NO + O_3 \rightarrow NO_2 + O_2 \quad (2)$$

$$NO_2 + O_3 \rightarrow NO_3 + O_2 \quad (3)$$

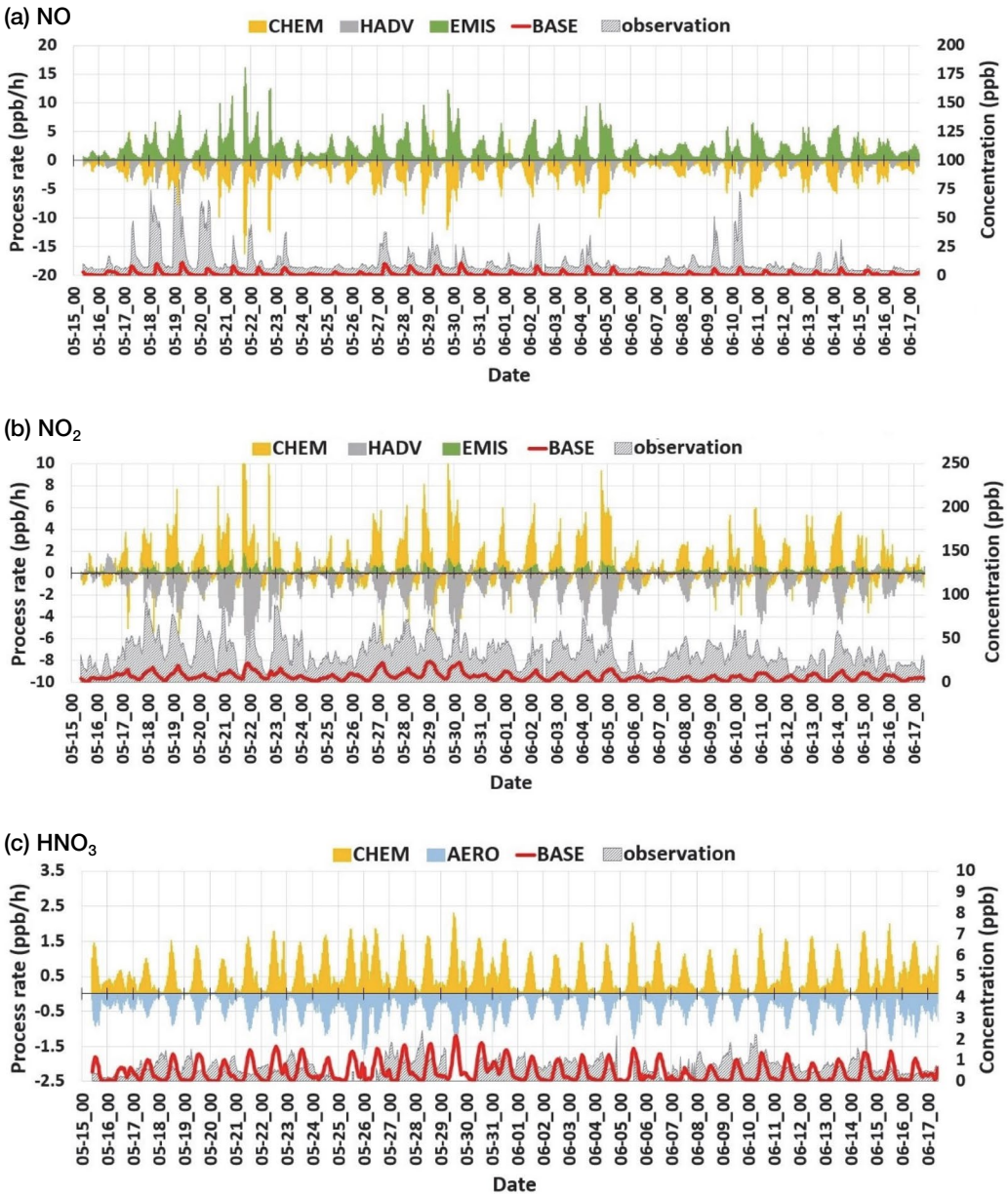

Fig. 4. OCABOX predictions and PA results of BASE run: (a) NO; (b) NO_2; (c) HNO_3; (d) NO_3^-; (e) NH_3; (f) NH_4^+.

$$NO_2 + NO_3 \rightarrow N_2O_5 \quad (4)$$

$$N_2O_5 + H_2O \rightarrow 2HNO_3 \quad (5)$$

When Reactions (2)–(5) are not important, HNO_3 reaches its maximum concentration during the day and minimum during the night in the presence of basic components (Mehlmann and Warneck, 1995), which can be attributed to the photochemical production during the day by Reaction (1) followed by its conversion to particulate NO_3^- during the night at high humidity and low temperature. A similar pattern is shown in the time series of the model-predicted HNO_3 concentration but the measured HNO_3 concentration did not show the nighttime minimum (Fig. 4c), particularly during the LRT period.

Fig. 5 shows the result of integrated reaction rate (IRR) analysis, which is the other part of PA, for HNO_3. The two pathways shown above were clearly distinguished in terms of the time of day and HNO_3 produc-

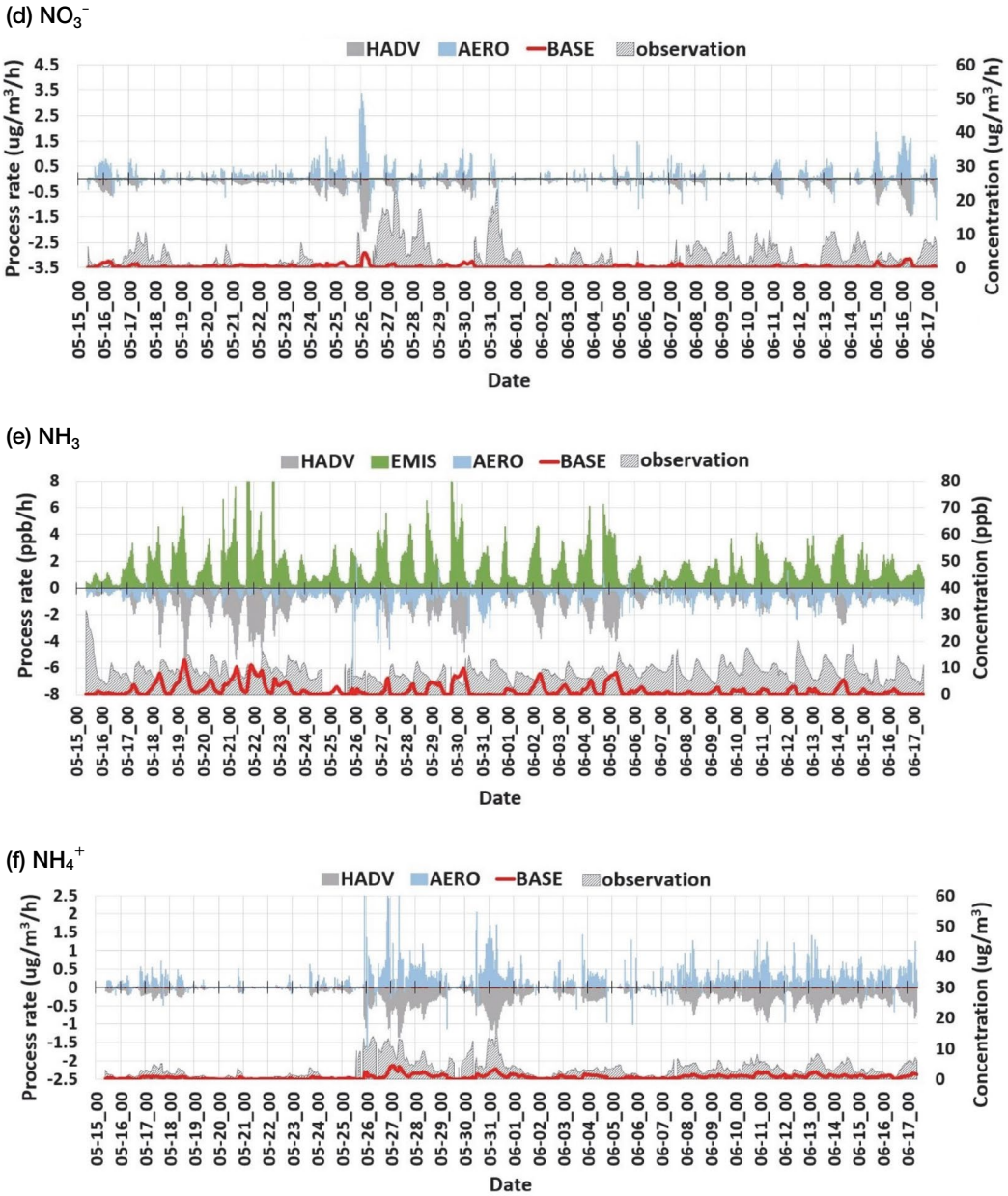

Fig. 4. Continued.

tion from N_2O_5 during the night was much weaker than that from OH during the day. The weak production of HNO_3 at night might be due to the low ozone concentration in the SMA with high NO_x emission. Subsection 3.4 will discuss the possibility of the transport of HNO_3 produced at night over the Yellow Sea located in the west of the SMA with abundant ozone because of little maritime NO_x emissions.

The underprediction of HNO_3 and NH_3 during the night and day, respectively, resulted in the corresponding underprediction of both NO_3^- and NH_4^+ (Fig. 4d and Fig. 4f) all day long throughout the simulation period. Several sensitivity analyses were performed to determine how the improved model prediction can be achieved.

3.2 Sensitivity Test Run 1 (SA1)

As shown in Fig. 4, the base run resulted in a general underestimation of NH_4^+ and NO_3^-, due to the underestimation of primary precursors NH_3, NO, and NO_2. This can be attributed to two possible reasons: underes-

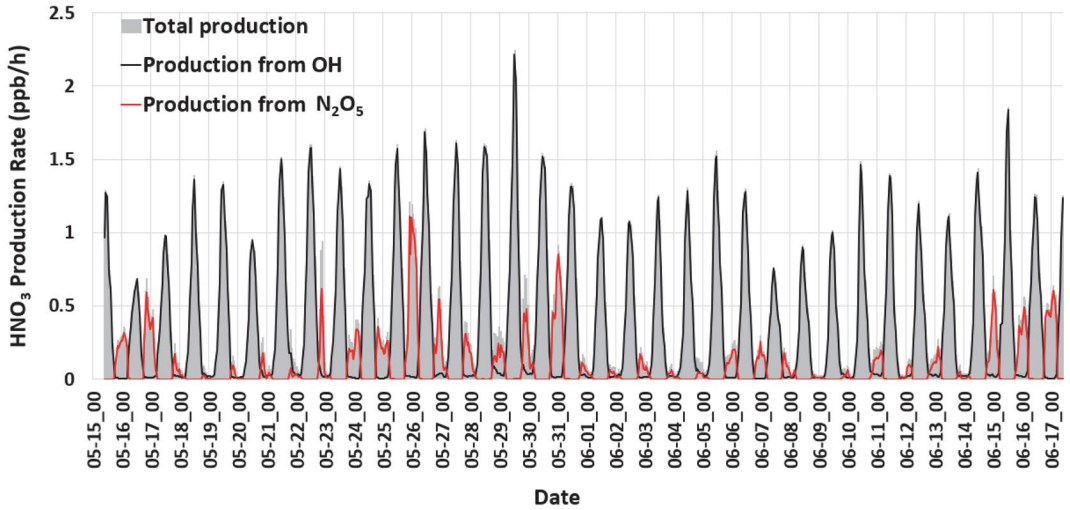

Fig. 5. HNO_3 production rates from the reactions with OH during the day and from the reactions with N_2O_5 during the night.

timated emissions and underestimated background concentrations.

A simple order-of-magnitude calculation based on the used emissions data showed the effects of the emissions to be ~0.1 ppb/h for both NH_3 and NO_x, which are too low to achieve the observed concentration levels. A previous study reported that even 50%-increased NO_x emissions led to an underestimation of the NO_x concentration in Seoul during the KORUS-AQ period (Oak *et al.*, 2019). On the other hand, the underestimated vehicle-emitted ammonia may lead to an underestimation of NH_4NO_3 (Link *et al.*, 2017). Therefore, the first sensitivity test conducted in this study was to increase NO, NO_2, and NH_3 emissions by a factor of 2 to see if this could reduce the gap between the model prediction and observation satisfactorily.

Fig. S2 shows the OCABOX predictions and PA results obtained with the doubled emissions of NO, NO_2, and NH_3. Simply doubling the emissions of the primary species did not improve the model performance very much. Although the NH_3 and HNO_3 concentrations were increased by emissions doubling, the underprediction of HNO_3 during the night and the underprediction of NH_3 during the day were not mitigated, resulting in a minor increase in the NH_4^+ and NO_3^- concentrations.

A possible reason why the increased emissions could not improve the model performance may be found by examining the free ammonia ratio (FAR) (Blanchard and Hidy, 2003):

$$\mathrm{FAR} = \frac{[\mathrm{NH_3}]^T - 2[\mathrm{SO_4}^{2-}]}{[\mathrm{HNO_3}]^T} \quad (6)$$

where $[\mathrm{NH_3}]^T = [\mathrm{NH_3}] + [\mathrm{NH_4}^+]$ and $[\mathrm{HNO_3}]^T = [\mathrm{HNO_3}] + [\mathrm{NO_3}^-]$ are the total ammonia and nitric acid molar concentrations, respectively. In the right-hand side of Eq. (6), the numerator means the amount of ammonia remaining after neutralizing $\mathrm{SO_4}^{2-}$. Therefore, FAR is the ratio of free ammonia over total nitric acid. If FAR > 1, the atmosphere is in an ammonia-rich condition. Fig. 6 shows the FAR values predicted by the BASE and SA1 runs with observed values. The observation gave the FAR values always larger than 1 (in the range of 1.27–138), often exceeding 10, except for the missing data, indicating an ammonia-rich condition that prevailed in SMA during the studied period. This is in agreement with the previous reports that total ammonia is in excess in the atmosphere of Seoul due to the local emissions from vehicles, agricultural activities, and industry (Kim *et al.*, 2018, 2017; Han and Kim, 2015; Kim, 2006). On the other hand, the model-predicted FAR values often decreased to below 1 for both BASE and SA1 runs, indicating that the model did not provide sufficient ammonia. The possibility of underestimating the emissions by more than a factor of 2 does not appear feasible. Therefore, additional sensitivity analyses needed to be conducted.

3.3 Sensitivity Test Run 2 (SA2)

In the second sensitivity analysis, NO, NO_2, NH_3, and

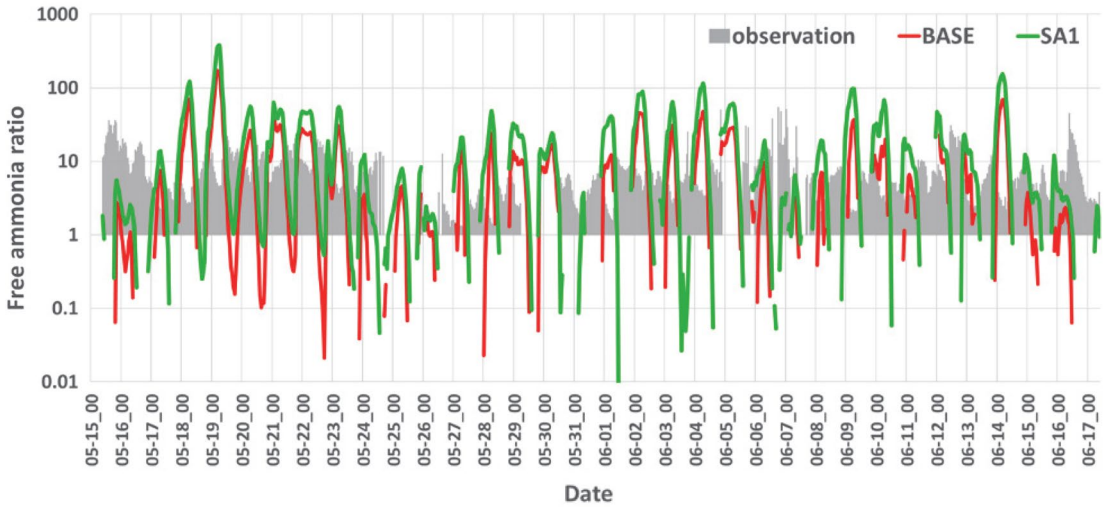

Fig. 6. Comparison of observed and OCABOX-predicted free ammonia ratios.

NH_4^+ were also constrained by the measurements (Table 3) to mitigate the effects of inaccurate emissions of NO_x and total ammonia. Fig. 7 and Fig. S3 (for NO and NO_2) present the results of the SA2 run. Although this led to naturally improved NH_3 and NH_4^+, NH_3 was overpredicted, while NH_4^+ was underpredicted, accompanied by an underprediction of HNO_3 and NO_3^- during the LRT period. This result can be interpreted as the excessive evaporation of NH_4^+ to NH_3 owing to the insufficient supply of HNO_3 by the model, again raising the possibility of the omission of HNO_3 transported from the Yellow Sea. On the other hand, the predictions of both NO_3^- and NH_4^+ were improved considerably during relatively short high PM event periods reportedly influenced by stagnant air (e.g., 7–8 June). Based on these results, it is important to test the hypothesis that the reason for the underprediction of nighttime total HNO_3 during the LRT period is due to the omission of the inflow of HNO_3 produced over the Yellow Sea.

3.4 Sensitivity Test Run 3 (SA3)

Until now, the data measured at the BI site (37.97°N, 124.63°E) for CO, O_3, SO_2, and NO_2 and the 'CMAQ profile' values for the other species were used as the boundary conditions for horizontal advection. Because the measured concentrations at the BI site and the CMAQ profile values are much lower than the concentrations in SMA except for O_3, the use of these boundary conditions may lead to strong ventilation for the box modeling, resulting in considerable underestimations. Therefore, two sensitivity tests were performed to account for the effects of polluted background.

The first test for the 'polluted background' hypothesis was conducted with respect to the possibility of the inflow of HNO_3 produced over the nearby Yellow Sea during the night. As was mentioned above, Reactions (2)–(5) are generally not crucial inside the SMA because the nighttime O_3 concentration tends to be low due to the active ozone titration by high NO emission. Over the Yellow Sea, which is located to the west of SMA, Reactions (2)–(5) can be significant because the maritime ozone tends to survive during the night due to negligible NO emission. If HNO_3 produced in this way flows into the SMA, where the ammonia-rich condition prevails, it may react efficiently with NH_3 to produce NH_4NO_3.

In SA3, all the measured data on relevant species (Na^+, K^+, Ca^{2+}, Mg^{2+}, Cl^-, HCl, SO_4^{2-}, NO_3^-, and NH_4^+) made at the BI site were added to the background field. The problem was that NH_3 and HNO_3 were not measured at the BI site. Therefore, their concentrations were estimated from the measured concentrations of NH_4^+ and NO_3^- as follows. First, the 3D model CMAQ was run, as described in Subsection 2.2. The average NH_3, HNO_3, NH_4^+, and NO_3^- concentrations for each hour during the whole period were calculated, and the average $[NH_3]/[NH_4^+]$ and $[HNO_3]/[NO_3^-]$ ratios were determined at each hour. Finally, the NH_3 and HNO_3 concentrations were estimated by multiplying these ratios by the measured concentrations of NH_4^+ and NO_3^-, respectively.

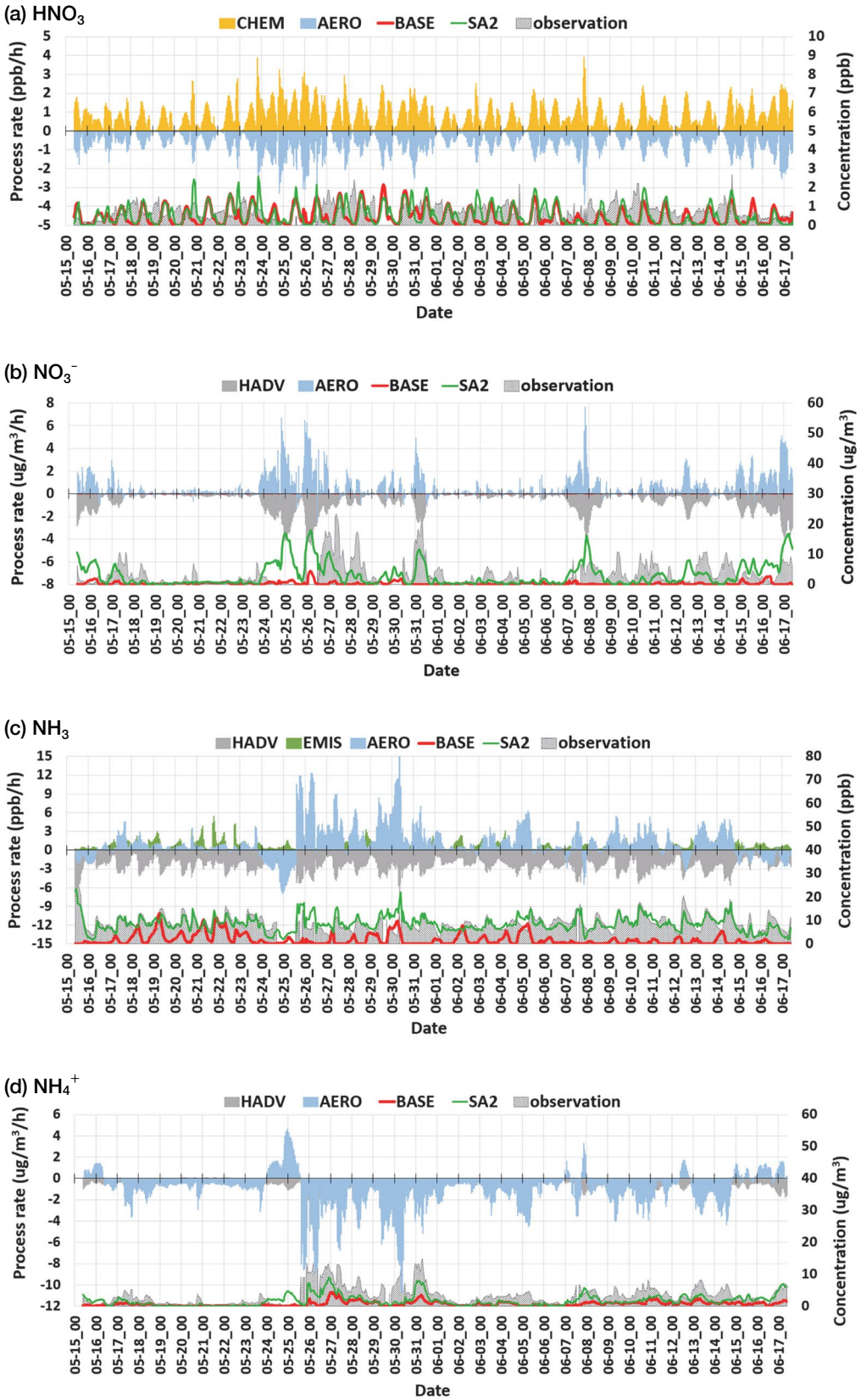

Fig. 7. OCABOX predictions and PA results of SA2 run: (a) HNO_3; (b) NO_3^-; (c) NH_3; (d) NH_4^+.

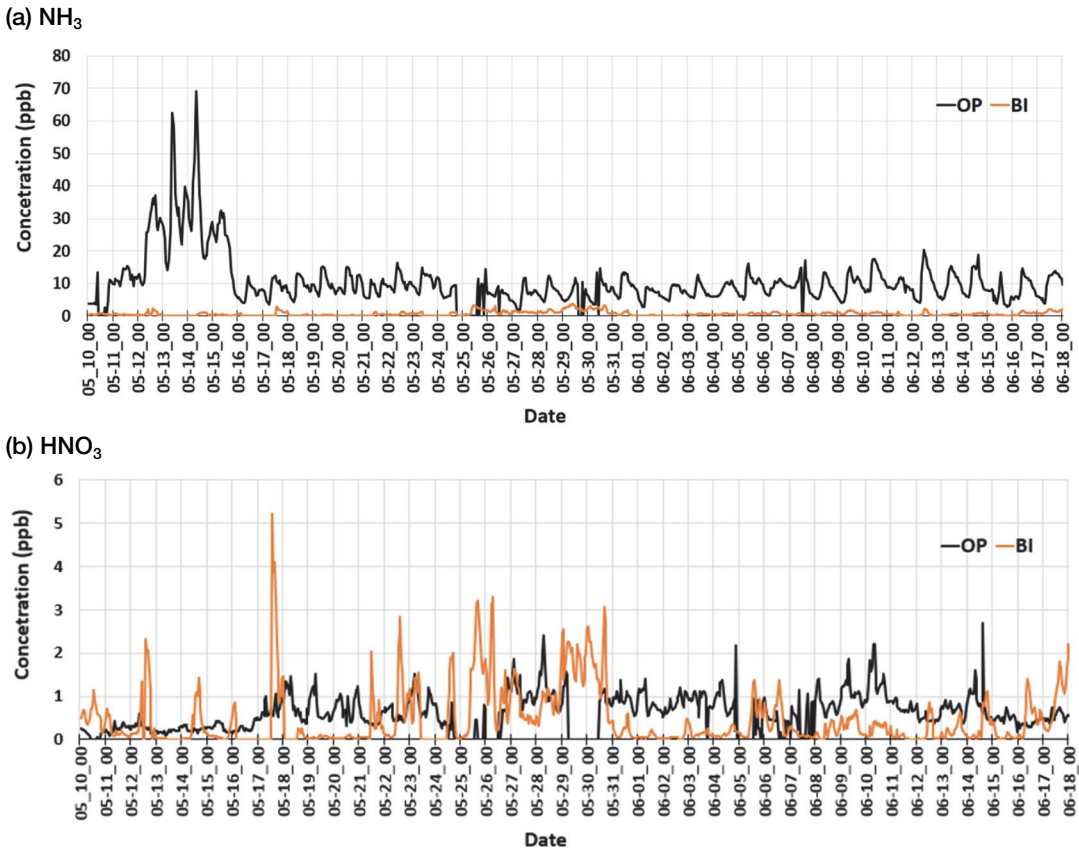

Fig. 8. Comparison of the concentrations measured at OP and BI sites: (a) NH_3; (b) HNO_3. The concentrations for the BI site were estimated using the measured $[NO_3^-]$ and $[NH_4^+]$ concentrations and the $[HNO_3]/[NO_3^-]$ and $[NH_3]/[NH_4^+]$ ratios predicted by CMAQ.

Fig. 8 compares the NH_3 and HNO_3 concentrations estimated in this way for the BI site with those measured at the OP site. The estimated BI NH_3 concentration was much lower than that measured at the OP site, as expected, because of the low NH_3 emission over the sea. On the other hand, the estimated BI HNO_3 concentration was as high as or even higher than the measured OP concentration during the LRT period. By contrast, during the non-LRT period, it was generally lower than the OP concentration. These results are very similar to the report of another research group who measured HNO_3 in both the BI and OP sites during the KORUS-AQ campaign (Korean Society for Atmospheric Environment, 2016).

Fig. 9 and Fig. S4 (for NO, NO_2, and NH_3) show the results of SA3. Despite the unchanged underestimation of NO and NO_2 compared to the BASE run, the HNO_3 and NO_3^- concentrations were increased significantly. This, in turn, led to considerable improvement in the prediction of high NH_4^+ concentrations during the LRT period. The degree of agreement with observation in terms of NH_4^+ concentration predicted for the LRT period was even better than SA2, in which NH_4^+ was constrained directly by observation. This result strongly suggests that the model-predicted NH_4NO_3 formation in that period was hindered by the shortage in supply of HNO_3 from the sea. On the other hand, the NH_4^+ prediction of SA3 during the non-LRT period was no better than that of SA2.

3.5 Sensitivity Test Run 4 (SA4)

SA4 was the last sensitivity analysis and the second test for polluted background. In this test, the effects of horizontal advection were removed. The SMA surrounding the box domain of this study is much larger than the box itself and usually maintains a high pollution level. Therefore, the air flowing into the box may have similar levels of pollutant concentrations, having little

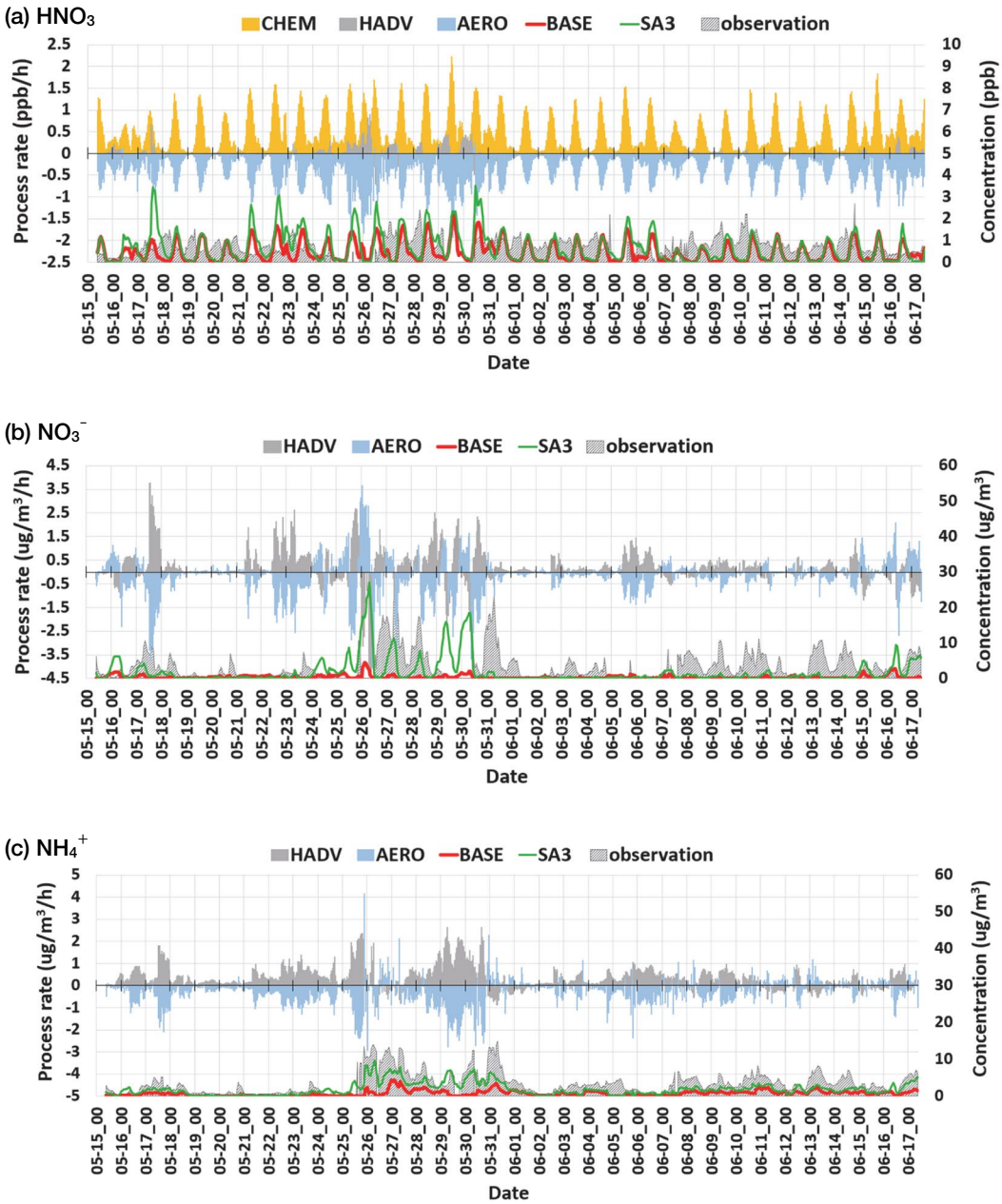

Fig. 9. OCABOX predictions and PA results of SA3 run: (a) HNO_3; (b) NO_3^-; (c) NH_4^+.

effect of horizontal advection.

In SA4, the background concentrations of NO, NO_2, NH_3, and NH_4^+, which may be influenced strongly by the emission sources in the vicinity, were replaced by the measured data at the OP site. This method was selected to incapacitate the ventilating effect of horizontal advection instead of simply skipping the horizontal advection process in the model because the latter may lead to the steady build-up of emitted primary pollutants in the box.

Fig. 10 presents the results of the SA4 run. The use of observations made at OP site as the regional background concentrations, without constraining them directly, led to accurate predictions of NO and NO_2, showing that the inflow from the polluted background is sufficient to maintain the high concentrations inside the box even without a large emission. This result suggests that the main reason for the underprediction of NO_x in the BASE run might not be the low emissions but the venti-

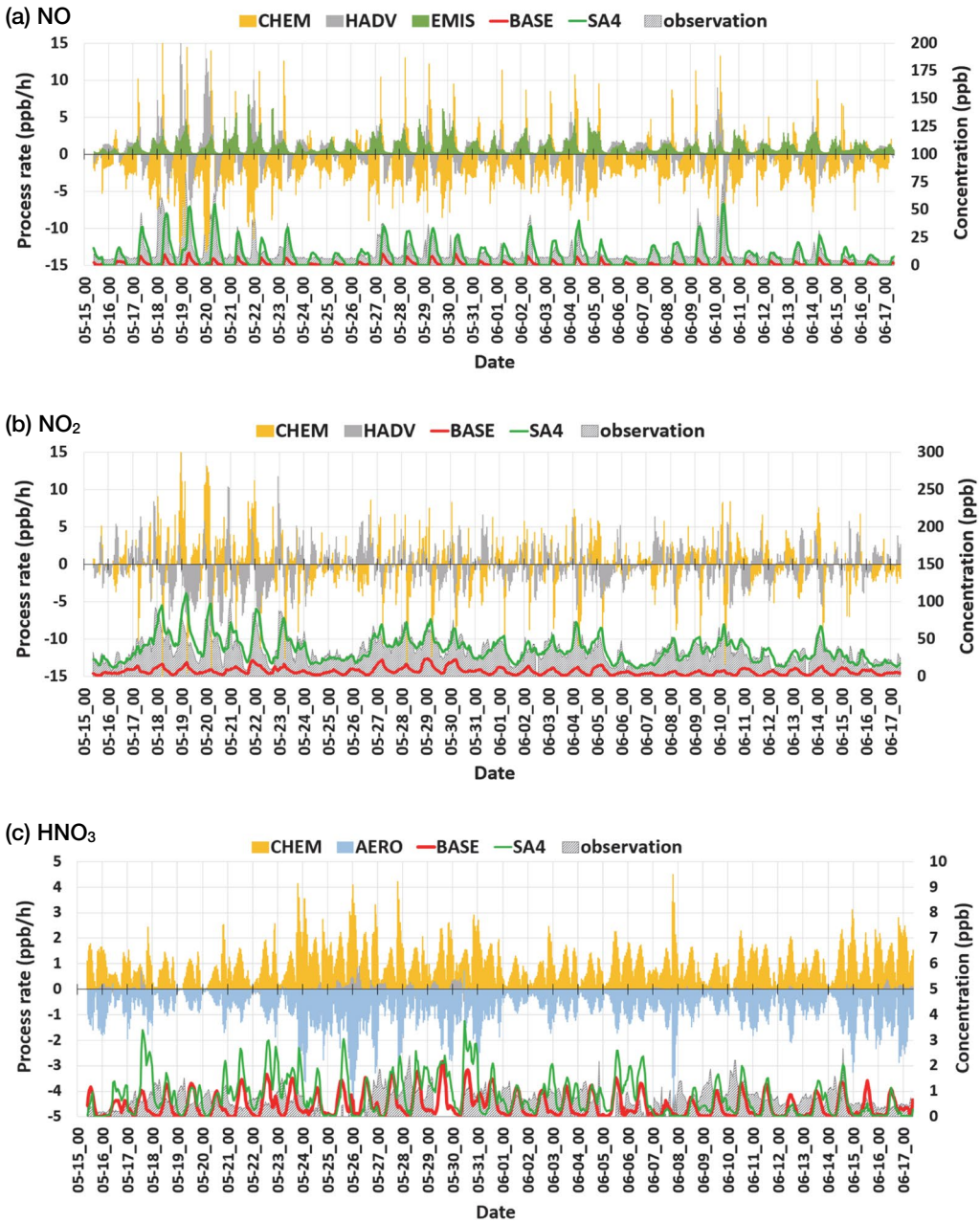

Fig. 10. OCABOX predictions and PA results of SA4 run: (a) NO; (b) NO_2; (c) HNO_3; (d) NO_3^-; (e) NH_3; (f) NH_4^+.

lation by unrealistically clean background air. The predictions for the concentrations of NH_3, HNO_3, NH_4^+, and NO_3^- all were improved for both the LRT and non-LRT periods because the supply of both the primary and secondary precursors from the regional background was accounted for.

The results of SA4 show that the assignment of appropriate regional background concentrations may be necessary for reliable box model predictions. For the secondary precursor HNO_3, for which nighttime production over the sea may be significant, the measurement made at the BI site appears adequate as the marine background condition, whereas the observations made inside the SMA may be better for the primary precursors, such as NO, NO_2, and NH_3. Overall, the box model OCA BOX can be a reliable tool for analyzing the formation of

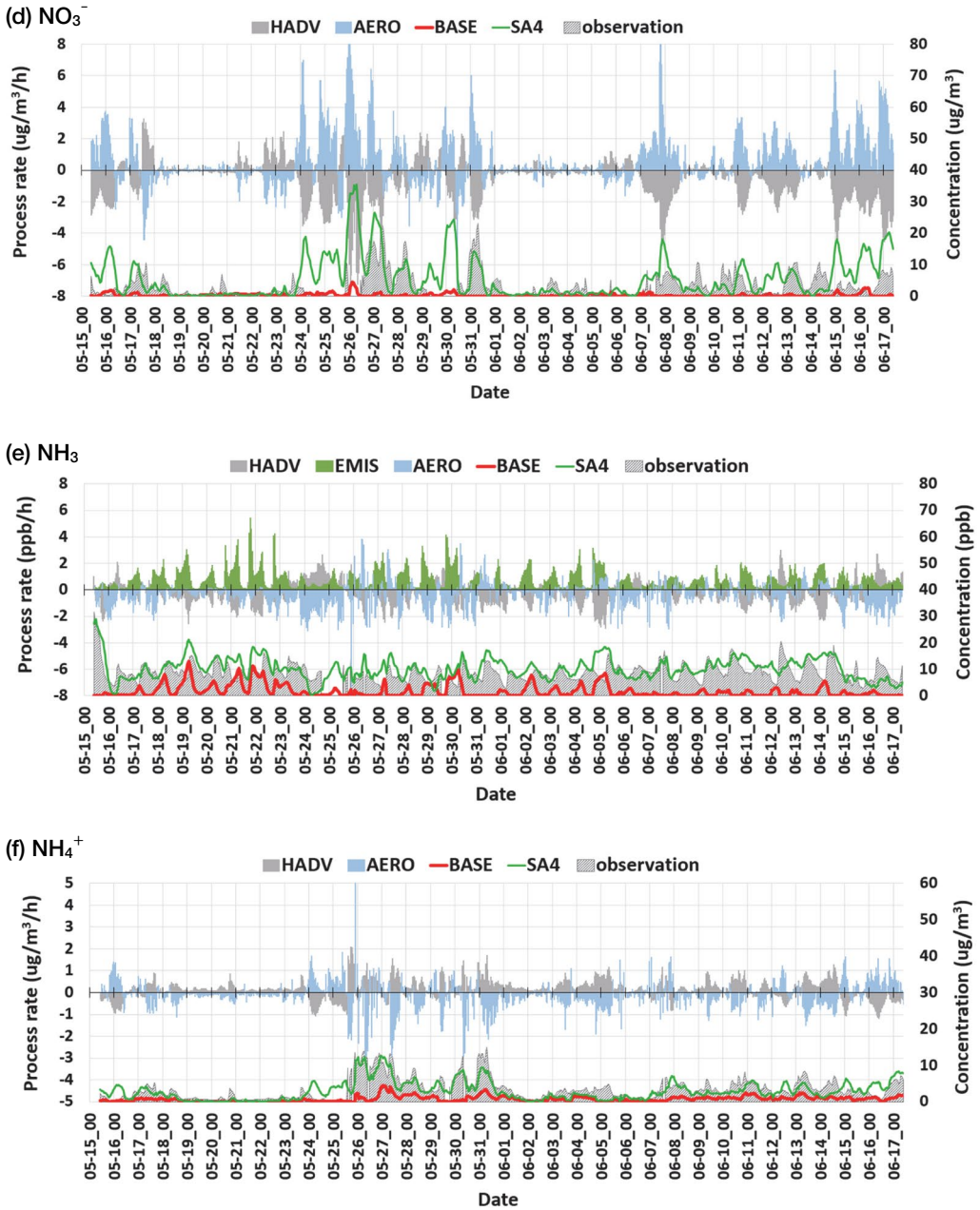

Fig. 10. Continued.

secondary inorganic aerosol if the assignment of regional background concentrations and the use of observation-based constraints are conducted appropriately. This conclusion needs to be verified by further investigations for the other high PM episodes in various regions in the future.

In order to show how the appropriate setting of boundary conditions can improve the model predictions, scatter plots comparing the NH_4^+ and NO_3^- concentrations predicted by the BASE and SA4 runs with observations are presented in Fig. 11. The statistic assessment results are summarized in Table 7. It is demonstrated by the scatter plots and statistical indices that the use of appropriate boundary conditions resolved the model underprediction of secondary inorganic PM species significantly.

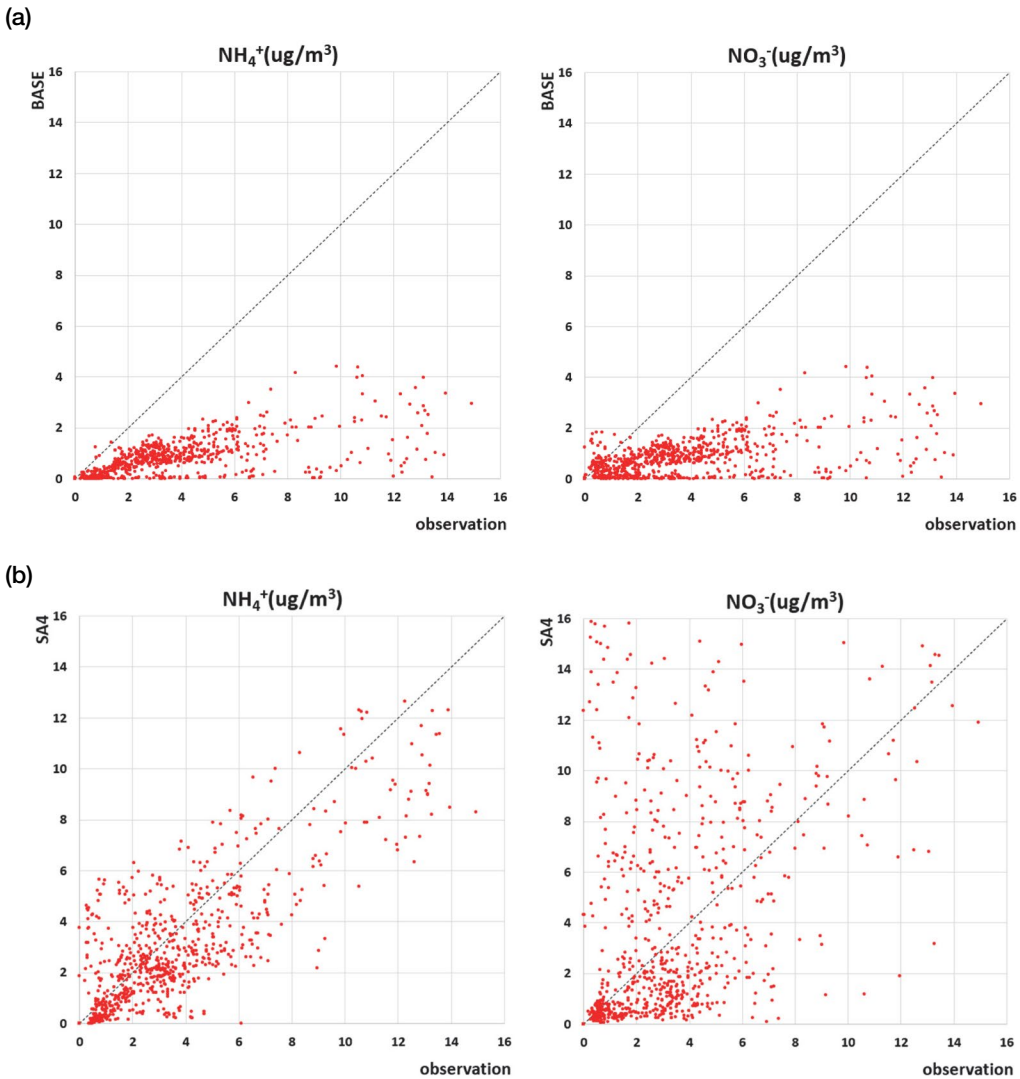

Fig. 11. Scatter plots comparing OCABOX predictions for NH_4^+ and NO_3^- with observations: (a) BASE run; (b) SA4.

Table 7. Statistical assessment of OCABOX predictions for NH_4^+ and NO_3^- concentrations ($\mu g/m^3$).

Simulations	Mean bias	Root mean square error	Index of agreement	Pearson correlation coefficient
Base NH_4^+	−2.692803615	3.678407564	0.495474196	0.64589919
SA4 NH_4^+	−0.561449207	1.885152294	0.885091202	0.791596972
Base NO_3^-	−2.812117037	3.872446803	0.435697945	0.518761307
SA4 NO_3^-	1.632027128	5.609523604	0.635156431	0.550501692

4. CONCLUSIONS

A box model OCABOX was used to study the formation of secondary inorganic aerosol in South Korea. A set of hourly data on major ionic components of $PM_{2.5}$ and their gaseous precursors measured at the Olympic Park ground site were used to run OCABOX and compare the simulation results. The measured data and simula-

tion results suggested that although the photochemical inland production during the day was the main pathway of the production of HNO_3 and NO_3^-, the maritime production during the night made nonnnegligible contribution during the LRT period. Appropriate regional background concentrations appeared to be essential for reliable box model simulation. The use of the observations made at a marine background site as the background concentrations could remedy the underestimation of HNO_3 by OCABOX. In the case of the primary precursors, the use of measurements made inside the SMA as background concentrations, without constraining them directly, led to better model performance.

ACKNOWLEDGEMENT

This research was supported by the National Institute of Environmental Research (NIER) of the Ministry of Environment of the Republic of Korea (grant No. NIER-2021-04-02-064).

REFERENCES

Abbatt, J., George, C., Melamed, M., Monks, P., Pandis, S., Rudich, Y. 2014. New directions: Fundamentals of atmospheric chemistry: Keeping a three-legged stool balanced. Atmospheric Environment, 84, 390–391.

Banks, R.F., Tiana-Alsina, J., Rocadenbosch, F., Baldasano, J.M. 2015. Performance evaluation of the boundary-layer height from lidar and the weather research and forecasting model at an urban coastal site in the north-east iberian peninsula. Boundary-Layer Meteorology, 157(2), 265–292.

Blanchard, C.L., Hidy, G.M. 2003. Effects of changes in sulfate, ammonia, and nitric acid on particulate nitrate concentrations in the southeastern united states. Journal of the Air & Waste Management Association, 53(3), 283–290.

Bloss, C., Wagner, V., Bonzanini, A., Jenkin, M.E., Wirtz, K., Martin-Reviejo, M., Pilling, M.J. 2005. Evaluation of detailed aromatic mechanisms (MCMv3 and MCMv3.1) against environmental chamber data. Atmospheric Chemistry and Physics, 5(3), 623–639.

Brauers, T., Hausmann, M., Bister, A., Kraus, A., Dorn, H.-P. 2001. OH radicals in the boundary layer of the atlantic ocean: 1. measurements by long-path laser absorption spectroscopy. Journal of Geophysical Research: Atmospheres, 106(D7), 7399–7414.

Brune, W.H., Baier, B.C., Thomas, J., Ren, X., Cohen, R.C., Pusede, S.E., Browne, E.C., Goldstein, A.H., Gentner, D.R., Keutsch, F.N. 2016. Ozone production chemistry in the presence of urban plumes. Faraday Discussions, 189, 169–189.

Burkholder, J.B., Abbatt, J.P.D., Barnes, I., Roberts, J.M., Melamed, M.L., Ammann, M., Bertram, A.K., Cappa, C.D., Carlton, A.G., Carpenter, L.J. 2017. The essential role for laboratory studies in atmospheric chemistry. Environmental Science & Technology, 51(5), 2519–2528.

Carslaw, N., Creasey, D.J., Heard, D.E., Lewis, A.C., McQuaid, J.B., Pilling, M.J., Monks, P.S., Bandy, B.J., Penkett, S.A. 1999. Modeling OH, HO_2, RO_2 radicals in the marine boundary layer: 1. model construction and comparison with field measurements. Journal of Geophysical Research: Atmospheres, 104(D23), 30241–30255.

Carter, W.P.L. 1995. Computer modeling of environmental chamber measurements of maximum incremental reactivities of volatile organic compounds. Atmospheric Environment, 29(18), 2513–2527.

Chen, G., Huey, L.G., Trainer, M., Nicks, D., Corbett, J., Ryerson, T., Parrish, D., Neuman, J.A., Nowak, J., Tanner, D. 2005. An investigation of the chemistry of ship emission plumes during ITCT 2002. Journal of Geophysical Research: Atmospheres, 110(D10), D10S90.

Chen, Y., Sexton, K.G., Jerry, R.E., Surratt, J.D., Vizuete, W. 2015. Assessment of SAPRC07 with updated isoprene chemistry against outdoor chamber experiments. Atmospheric Environment, 105, 109–120.

Choi, E.-K., Kim, Y.-P. 2010. Effects of aerosol hygroscopicity on fine particle mass concentration and light extinction coefficient at Seoul and Gosan in Korea. Asian Journal of Atmospheric Environment, 4(1), 55–61.

Choi, J.C., Lee, M., Chun, Y., Kim, J., Oh, S. 2001. Chemical composition and source signature of spring aerosol in Seoul, Korea. Journal of Geophysical Research: Atmospheres, 106(D16), 18067–18074.

Choi, J., Park, R.J., Lee, H.-M., Lee, S., Jo, D.S., Jeong, J.I., Henze, D.K., Woo, J.-H., Ban, S.-J., Lee, M.-D. 2019. Impacts of local vs. trans-boundary emissions from different sectors on $PM_{2.5}$ exposure in South Korea during the KORUS-AQ campaign. Atmospheric Environment, 203, 196–205.

Crawford, J.H., Ahn, J.-Y., Al-Saadi, J., Chang, L., Emmons, L.K., Kim, J., Lee, G., Park, J.-H., Park, R.J., Woo, J.H. 2021. The Korea-United states air quality (KORUS-AQ) field study. Elementa: Science of the Anthropocene, 9(1), 00163.

Edwards, P.M., Brown, S.S., Roberts, J.M., Ahmadov, R., Banta, R.M., Degouw, J.A., Dube, W.P., Field, R.A., Flynn, J.H., Gilman, J.B. 2014. High winter ozone pollution from carbonyl photolysis in an oil and gas basin. Nature, 514(7522), 351–354.

Eisele, F.L., Mount, G.H., Fehsenfeld, F.C., Harder, J., Marovich, E., Parrish, D.D., Roberts, J., Trainer, M., Tanner, D. 1994. Intercomparison of tropospheric OH and ancillary trace gas measurements at fritz peak observatory, colorado. Journal of Geophysical Research: Atmospheres, 99(D9), 18605–18626.

Elshorbany, Y.F., Kurtenbach, R., Wiesen, P., Lissi, E., Rubio, M., Villena, G., Gramsch, E., Rickard, A.R., Pilling, M.J., Kleffmann, J. 2009. Oxidation capacity of the city air of santiago, chile. Atmospheric Chemistry and Physics 9(6), 2257–2273.

Emmerson, K.M., Carslaw, N., Carslaw, D.C., Lee, J.D., McFiggans, G., Bloss, W.J., Gravestock, T., Heard, D.E., Hopkins, J., Ingham, T. 2007. Free radical modelling studies during the UK TORCH campaign in summer 2003. Atmospheric Chemistry and Physics, 7(1), 167–181.

Ghosh, S., Shon, Z.-H., Kim, K.-H., Song, S.-K., Jung, K., Kim, N.-J. 2012. Seasonal variation of $PM_{2.5}$ and its major ionic components in an urban monitoring site. Asian Journal of Atmospheric Environment, 6(1), 23–32.

Han, S.H., Kim, Y.P. 2015. Long-term trends of the concentrations of mass and chemical composition in $PM_{2.5}$ over Seoul. Journal of Korean Society for Atmospheric Environment, 31(2), 143–156.

He, Y., Uno, I., Wang, Z., Ohara, T., Sugimoto, N., Shimizu, A., Richter, A., Burrows, J.P. 2007. Variations of the increasing trend of tropospheric NO_2 over central east china during the past decade. Atmospheric Environment, 41(23), 4865–4876.

Jordan, C.E., Crawford, J.H., Beyersdorf, A.J., Eck, T.F., Halliday, H.S., Nault, B.A., Chang, L.-S., Park, J., Park, R., Lee, G. 2020. Investigation of factors controlling $PM_{2.5}$ variability across the South Korean peninsula during KORUS-AQ. Elementa: Science of the Anthropocene, 8, 28.

Kang, C.-M., Kang, B.-W., Lee, H.S. 2006. Source identification and trends in concentrations of gaseous and fine particulate principal species in Seoul, South Korea. Journal of the Air & Waste Management Association, 56(7), 911–921.

Kang, C.-M., Lee, H.S., Kang, B.-W., Lee, S.-K., Sunwoo, Y. 2004. Chemical characteristics of acidic gas pollutants and $PM_{2.5}$ species during hazy episodes in Seoul, South Korea. Atmospheric Environment, 38(28), 4749–4760.

Kim, H., Zhang, Q., Bae, G.-N., Kim, J.Y., Lee, S.B. 2017. Sources and atmospheric processing of winter aerosols in Seoul, Korea: Insights from real-time measurements using a high-resolution aerosol mass spectrometer. Atmospheric Chemistry and Physics, 17(3), 2009–2033.

Kim, H., Zhang, Q., Heo, J. 2018. Influence of intense secondary aerosol formation and long-range transport on aerosol chemistry and properties in the Seoul metropolitan area during spring time: Results from KORUS-AQ. Atmospheric Chemistry and Physics, 18(10), 7149–7168.

Kim, N.G., Kim, Y.P., Kang, C.H., Moon, K.-C. 2004. Characteristics of nitrate concentration measured at gosan: Measurement data of $PM_{2.5}$ and TSP between 1998 and 2002. Journal of Korean Society for Atmospheric Environment, 20(1), 119–128.

Kim, Y.P., Lee, G. 2018. Trend of air quality in Seoul: Policy and science. Aerosol and Air Quality Research, 18(9), 2141–2156.

Kim, Y.-P. 2006. Air pollution in Seoul caused by aerosols. Journal of Korean Society for Atmospheric Environment, 22(5), 535–553.

Kim, Y., Kim, S.-W., Yoon, S.-C., Kim, M.-H., Park, K.-H. 2014. Aerosol properties and associated regional meteorology during winter pollution event at gosan climate observatory, Korea. Atmospheric Environment, 85, 9–17.

Kim, Y., Park, O., Park, S.H., Kim, M.J., Kim, J.-J., Choi, J.-Y., Lee, D., Cho, S., Shim, S. 2022. $PM_{2.5}$ pH estimation in Seoul during the KORUS-AQ campaign using different thermodynamic models. Atmospheric Environment, 268, 118787.

Korean Society for Atmospheric Environment. 2016. Characterization on the distribution of particulate matter during KORUS-AQ campaign (in Korean). NIER-SP2016-181.

Lee, B.K., Kim, Y.H., Ha, J.Y., Lee, D.S. 2005. Development of an automated and continuous analysis system for $PM_{2.5}$ and chemical characterization of the $PM_{2.5}$ in the atmosphere at Seoul. Journal of Korean Society for Atmospheric Environment, 21(4), 439–458.

Lee, Y.H., Choi, Y., Ghim, Y.S. 2016. Classification of diurnal patterns of particulate inorganic ions downwind of metropolitan Seoul. Environmental Science and Pollution Research, 23(9), 8917–8928.

Link, M.F., Kim, J., Park, G., Lee, T., Park, T., Babar, Z.B., Sung, K., Kim, P., Kang, S., Kim, J.S. 2017. Elevated production of NH_4NO_3 from the photochemical processing of vehicle exhaust: Implications for air quality in the Seoul metropolitan region. Atmospheric Environment, 156, 95–101.

Lu, K.D., Rohrer, F., Holland, F., Fuchs, H., Bohn, B., Brauers, T., Chang, C.C., Häseler, R., Hu, M., Kita, K. 2012. Observation and modelling of OH and HO_2 concentrations in the pearl river delta 2006: A missing OH source in a VOC rich atmosphere. Atmospheric Chemistry and Physics, 12(3), 1541–1569.

Mehlmann, A., Warneck, P. 1995. Atmospheric gaseous HNO_3, particulate nitrate, and aerosol size distributions of major ionic species at a rural site in western germany. Atmospheric Environment, 29(17), 2359–2373.

Meng, Z., Dabdub, D., Seinfeld, J.H. 1997. Chemical coupling between atmospheric ozone and particulate matter. Science, 277(5322), 116–119.

Metzger, A., Dommen, J., Gaeggeler, K., Duplissy, J., Prevot, A.S.H., Kleffmann, J., Elshorbany, Y., Wisthaler, A., Baltensperger, U. 2008. Evaluation of 1, 3, 5 trimethylbenzene degradation in the detailed tropospheric chemistry mechanism, MCMv3.1, using environmental chamber data. Atmospheric Chemistry and Physics, 8(21), 6453–6468.

National Institute of Environmental Research. National air pollutants emission service. 2019 [cited 24 November 2021]. Available from http://airemiss.nier.go.kr/mbshome/mbs/airemiss/index.do.

National Institute of Environmental Research and National Aeronautics and Space Administration. 2017. KORUS-AQ rapid science synthesis report.

Nault, B.A., Campuzano-Jost, P., Day, D.A., Schroder, J.C., Anderson, B., Beyersdorf, A.J., Blake, D.R., Brune, W.H., Choi, Y., Corr, C.A. 2018. Secondary organic aerosol production from local emissions dominates the organic aerosol budget over Seoul, South Korea, during KORUS-AQ. Atmospheric Chemistry and Physics, 18(24), 17769–17800.

Novelli, A., Kaminski, M., Rolletter, M., Acir, I.-H., Bohn, B., Dorn, H.-P., Li, X., Lutz, A., Nehr, S., Rohrer, F. 2018. Evaluation of OH and HO_2 concentrations and their budgets during photooxidation of 2-methyl-3-butene-2-ol (MBO) in the atmospheric simulation chamber SAPHIR. Atmospheric Chemistry and Physics, 18(15), 11409–11422.

Oak, Y.J., Park, R.J., Schroeder, J.R., Crawford, J.H., Blake, D.R.,

Weinheimer, A.J., Woo, J.-H., Kim, S.-W., Yeo, H., Fried, A. 2019. Evaluation of simulated O_3 production efficiency during the KORUS-AQ campaign: Implications for anthropogenic NO_x emissions in Korea. Elementa: Science of the Anthropocene, 7, 56.

Ocskay, R., Salma, I., Wang, W., Maenhaut, W. 2006. Characterization and diurnal variation of size-resolved inorganic water-soluble ions at a rural background site. Journal of Environmental Monitoring, 8(2), 300–306.

Park, R.J., Oak, Y.J., Emmons, L.K., Kim, C.-H., Pfister, G.G., Carmichael, G.R., Saide, P.E., Cho, S.-Y., Kim, S., Woo, J.-H. 2021. Multi-model intercomparisons of air quality simulations for the KORUS-AQ campaign. Elementa: Science of the Anthropocene, 9(1).

Park, S.S., Kim, Y.J. 2004. $PM_{2.5}$ particles and size-segregated ionic species measured during fall season in three urban sites in Korea. Atmospheric Environment, 38(10), 1459–1471.

Park, S.-S., Jung, S.-A., Gong, B.-J., Cho, S.-Y., Lee, S.-J. 2013. Characteristics of $PM_{2.5}$ haze episodes revealed by highly time-resolved measurements at an air pollution monitoring supersite in Korea. Aerosol and Air Quality Research, 13(3), 957–976.

Peterson, D.A., Hyer, E.J., Han, S.-O., Crawford, J.H., Park, R.J., Holz, R., Kuehn, R.E., Eloranta, E., Knote, C., Jordan, C.E. 2019. Meteorology influencing springtime air quality, pollution transport, and visibility in Korea. Elementa: Science of the Anthropocene, 7, 57.

Powers, J.G., Klemp, J.B., Skamarock, W.C., Davis, C.A., Dudhia, J., Gill, D.O., Coen, J.L., Gochis, D.J., Ahmadov, R., Peckham, S.E. 2017. The weather research and forecasting model: Overview, system efforts, and future directions. Bulletin of the American Meteorological Society, 98 (8), 1717–1737.

Ren, X., Olson, J.R., Crawford, J.H., Brune, W.H., Mao, J., Long, R.B., Chen, Z., Chen, G., Avery, M.A., Sachse, G.W. 2008. HO_x chemistry during INTEX-A 2004: Observation, model calculation, and comparison with previous studies. Journal of Geophysical Research: Atmospheres, 113(D5), D05310.

Richter, A., Burrows, J.P., Nüß, H., Granier, C., Niemeier, U. 2005. Increase in tropospheric nitrogen dioxide over china observed from space. Nature, 437(7055), 129–132.

Ro, C.-U., Oh, K.-Y., Kim, H., Kim, Y.P., Lee, C.B., Kim, K.-H., Kang, C.H., János, O., de Hoog, J., Worobiec, A., Grieken, R.V. 2001. Single-particle analysis of aerosols at cheju island, Korea, using low-Z electron probe X-ray microanalysis: A direct proof of nitrate formation from sea salts. Environmental Science & Technology, 35(22), 4487–4494.

Savoie, D.L., Prospero, J.M. 1982. Particle size distribution of nitrate and sulfate in the marine atmosphere. Geophysical Research Letters, 9(10), 1207–1210.

Schroeder, J.R., Crawford, J.H., Ahn, J.-Y., Chang, L., Fried, A., Walega, J., Weinheimer, A., Montzka, D.D., Hall, S.R., Ullmann, K. 2020. Observation-based modeling of ozone chemistry in the Seoul metropolitan area during the Korea-united states air quality study (KORUS-AQ). Elementa: Science of the Anthropocene, 8, 3.

Seinfeld, J.H., Pandis, S.N. 2016. Atmospheric chemistry and physics: From air pollution to climate change. 3rd Ed. ed. Hoboken, New Jersey: John Wiley & Sons.

Shon, Z.-H., Kim, K.-H., Song, S.-K., Jung, K., Kim, N.-J., Lee, J.-B. 2012. Relationship between water-soluble ions in $PM_{2.5}$ and their precursor gases in Seoul megacity. Atmospheric Environment, 59, 540–550.

Sommariva, R., De Gouw, J.A., Trainer, M., Atlas, E., Goldan, P.D., Kuster, W.C., Warneke, C., Fehsenfeld, F.C. 2011a. Emissions and photochemistry of oxygenated VOCs in urban plumes in the northeastern united states. Atmospheric Chemistry and Physics, 11(14), 7081–7096.

Sommariva, R., Osthoff, H.D., Brown, S.S., Bates, T.S., Baynard, T., Coffman, D., De Gouw, J.A., Goldan, P.D., Kuster, W.C., Lerner, B.M. 2009. Radicals in the marine boundary layer during NEAQS 2004: A model study of day-time and night-time sources and sinks. Atmospheric Chemistry and Physics, 9(9), 3075–3093.

Sommariva, R., Bates, T.S., Bon, D., Brookes, D.M., de Gouw, J.A., Gilman, J.B., Herndon, S.C., Kuster, W.C., Lerner, B.M., Monks, P.S. 2011b. Modelled and measured concentrations of peroxy radicals and nitrate radical in the US gulf coast region during TexAQS 2006. Journal of Atmospheric Chemistry, 68(4), 331–362.

Sommariva, R., Cox, S., Martin, C., Borońska, K., Young, J., Jimack, P.K., Pilling, M.J., Matthaios, V.N., Nelson, B.S., Newland, M.J. 2020. AtChem (version 1), an open-source box model for the master chemical mechanism. Geoscientific Model Development, 13(1), 169–183.

Sommariva, R., Trainer, M., de Gouw, J.A., Roberts, J.M., Warneke, C., Atlas, E., Flocke, F., Goldan, P.D., Kuster, W.C., Swanson, A.L. 2008. A study of organic nitrates formation in an urban plume using a master chemical mechanism. Atmospheric Environment, 42(23), 5771–5786.

Song, C.H., Chen, G., Hanna, S.R., Crawford, J., Davis, D.D. 2003. Dispersion and chemical evolution of ship plumes in the marine boundary layer: Investigation of $O_3/NO_y/HO_x$ chemistry. Journal of Geophysical Research: Atmospheres, 108(D4), 4143.

von Glasow, R., Lawrence, M.G., Sander, R., Crutzen, P.J. 2003. Modeling the chemical effects of ship exhaust in the cloud-free marine boundary layer. Atmospheric Chemistry and Physics, 3(1), 233–250.

Wang, Y., Tang, G., Zhao, W., Yang, Y., Wang, L., Liu, Z., Wen, T., Cheng, M., Wang, Y., Wang, Y. 2020. Different roles of nitrate and sulfate in air pollution episodes in the north china plain. Atmospheric Environment, 224, 117325.

Whalley, L.K., Stone, D., Bandy, B., Dunmore, R., Hamilton, J.F., Hopkins, J., Lee, J.D., Lewis, A.C., Heard, D.E. 2016. Atmospheric OH reactivity in central london: Observations, model predictions and estimates of in situ ozone production. Atmospheric Chemistry and Physics, 16(4), 2109–2122.

Wolfe, G.M., Marvin, M.R., Roberts, S.J., Travis, K.R., Liao, J. 2016. The framework for 0-D atmospheric modeling (F0AM) v3.1. Geoscientific Model Development, 9(9), 3309–3319.

Wolff, G.T. 1984. On the nature of nitrate in coarse continental aerosols. Atmospheric Environment, 18(5), 977–981.

Xue, J., Yuan, Z., Lau, A.K.H., Yu, J.Z. 2014. Insights into factors affecting nitrate in $PM_{2.5}$ in a polluted high NO_x envi-

ronment through hourly observations and size distribution measurements. Journal of Geophysical Research: Atmospheres, 119(8), 4888–4902.
Yarwood, G., Jung, J., Whitten, G.Z., Heo, G., Mellberg, J., Estes, M. 2010. Updates to the carbon bond mechanism for version 6 (CB6). Paper presented at 9th Annual CMAS Conference, 11–13 October 2010, Chapel Hill, NC.

SUPPLEMENTARY MATERIALS

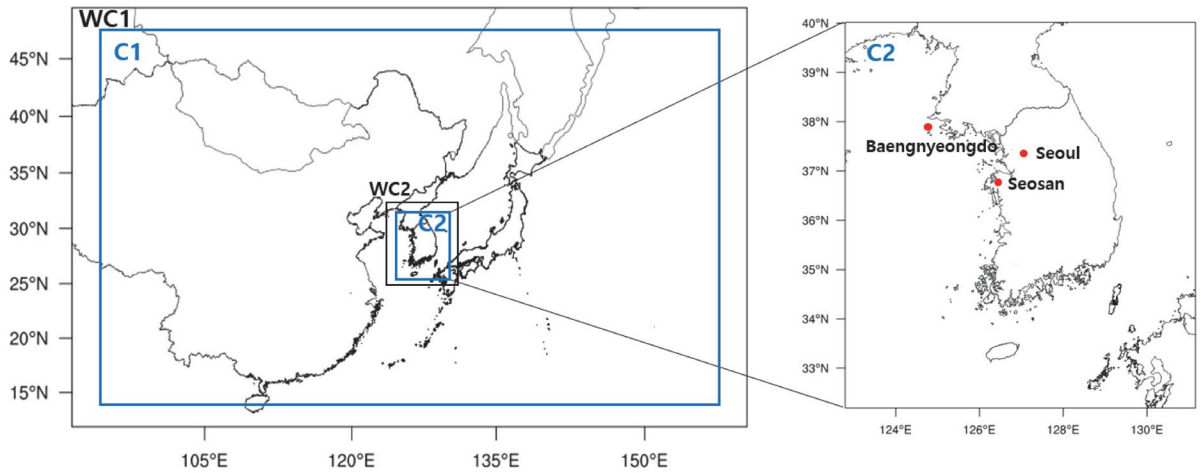

Fig. S1. The spatial domains used for the sensitivity test on the background concentrations.

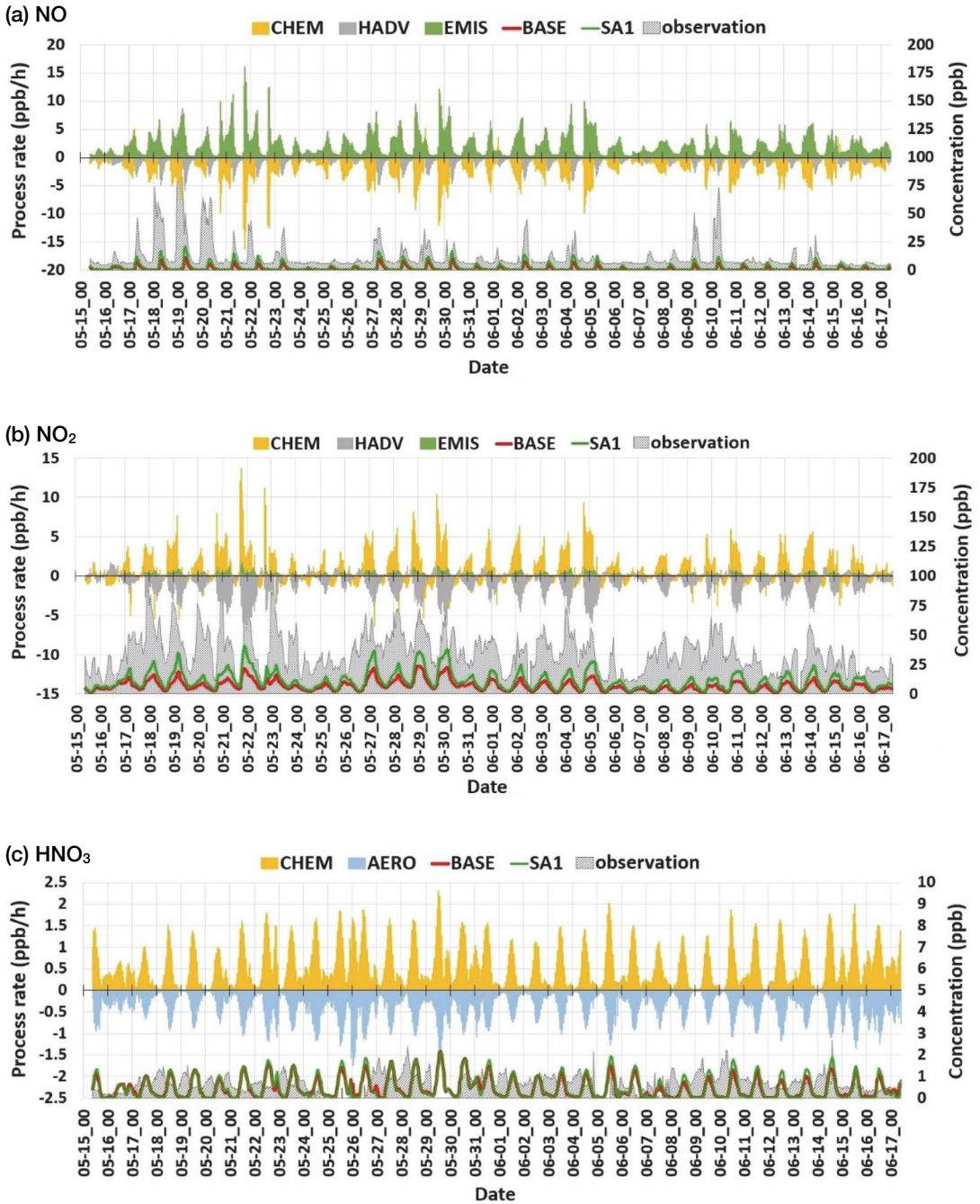

Fig. S2. OCABOX predictions and PA results of SA1 run: (a) NO; (b) NO_2; (c) HNO_3; (d) NO_3^-; (e) NH_3; (f) NH_4^+.

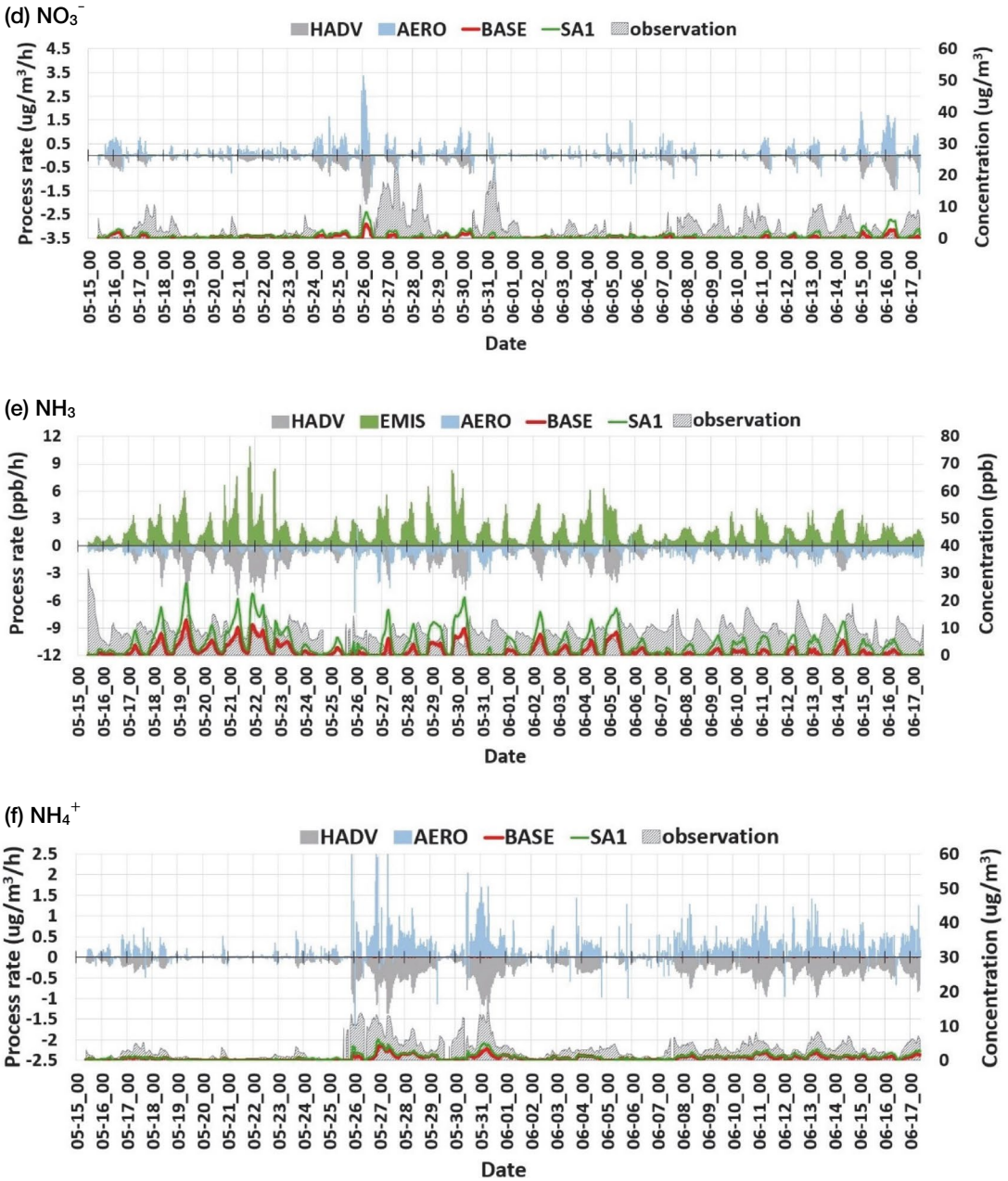

Fig. S2. Continued.

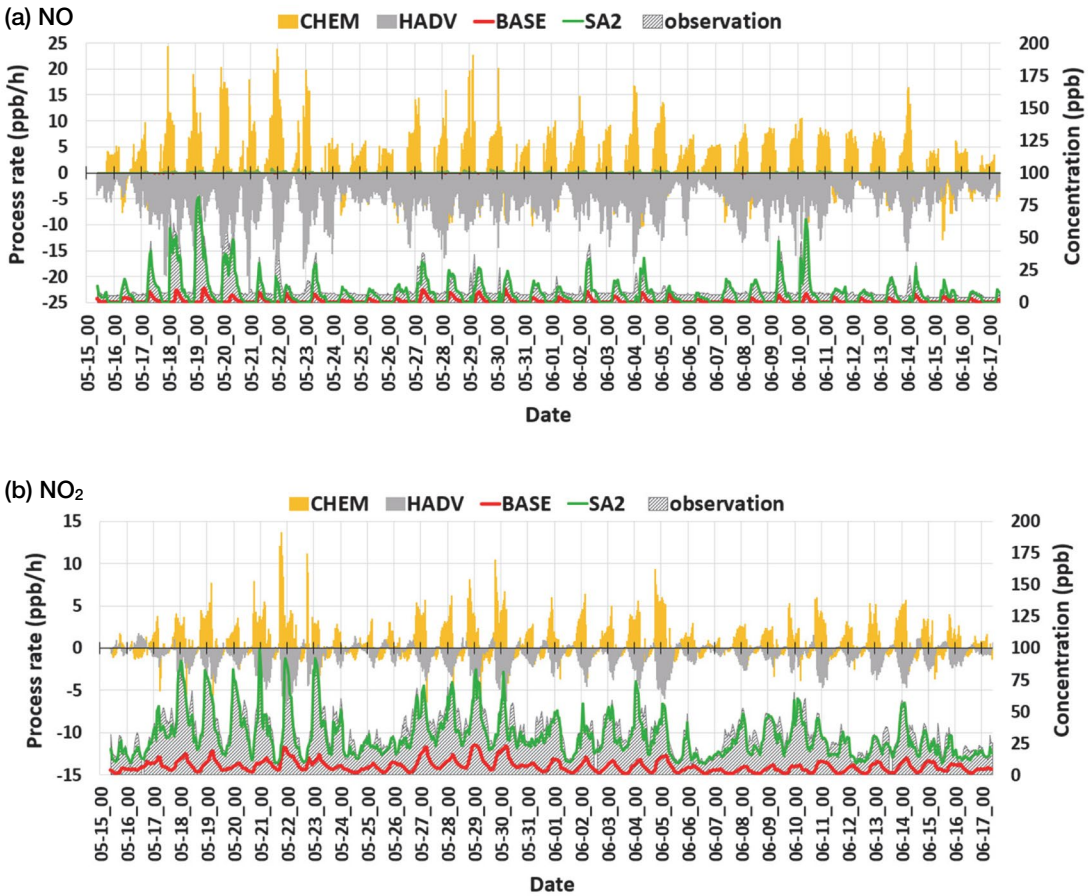

Fig. S3. OCABOX predictions and PA results of SA2 run: (a) NO; (b) NO_2.

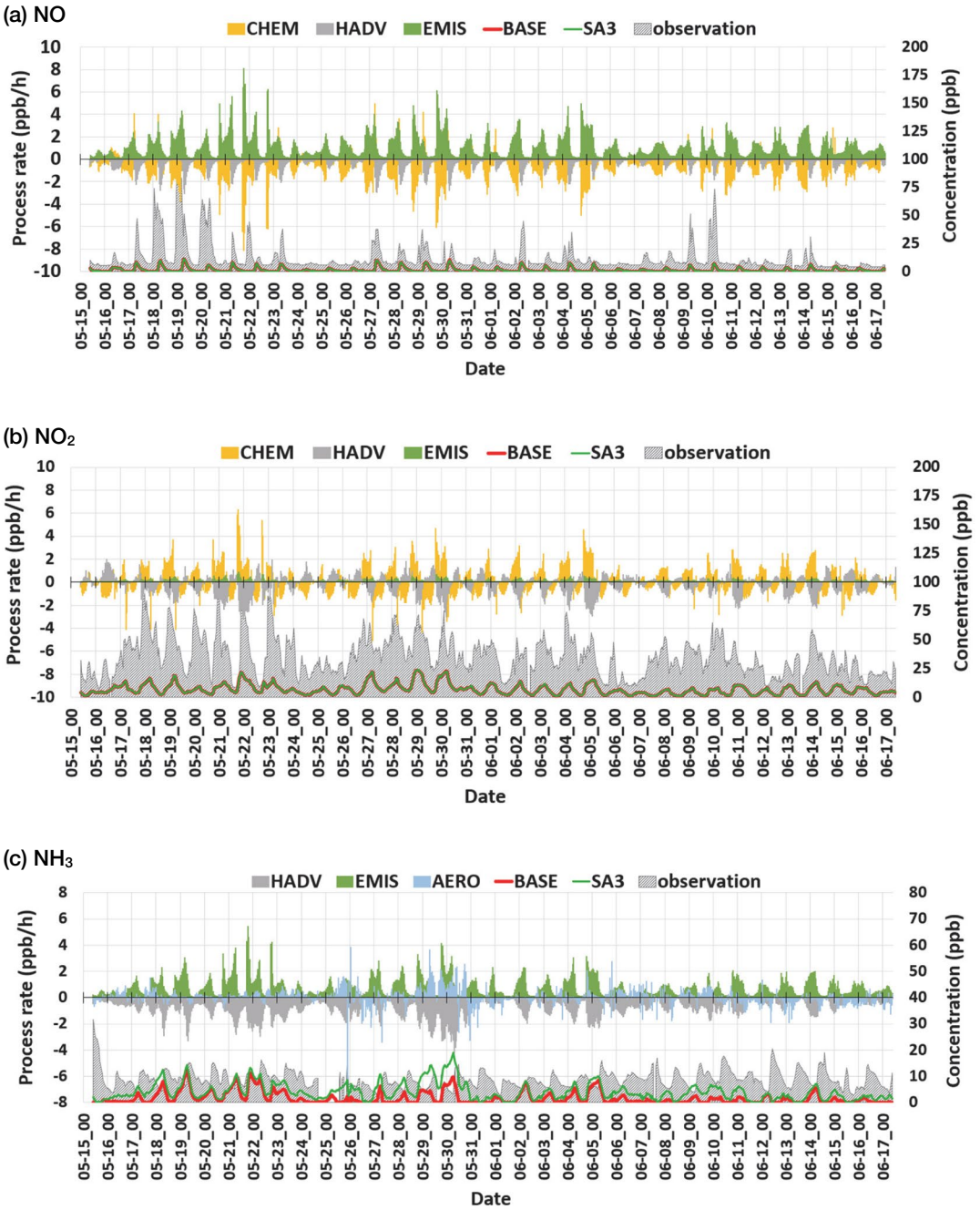

Fig. S4. OCABOX predictions and PA results of SA3 run: (a) NO; (b) NO_2; (c) NH_3.